The Astrophysical Journal Letters, 915:L5 (24pp), 2021 July 1 https://doi.org/10.3847/2041-8213/ac082e

Observation of Gravitational Waves from Two Neutron Star–Black Hole Coalescences

R. Abbott[1], T. D. Abbott[2], S. Abraham[3], F. Acernese[4,5], K. Ackley[6], A. Adams[7], C. Adams[8], R. X. Adhikari[1], V. B. Adya[9], C. Affeldt[10,11], D. Agarwal[3], M. Agathos[12,13], K. Agatsuma[14], N. Aggarwal[15], O. D. Aguiar[16], L. Aiello[17,18,19], A. Ain[20,21], P. Ajith[22], T. Akutsu[23,24], K. M. Aleman[25], G. Allen[26], A. Allocca[5,27], P. A. Altin[9], A. Amato[28], S. Anand[1], A. Ananyeva[1], S. B. Anderson[1], W. G. Anderson[29], M. Ando[30,31], S. V. Angelova[32], S. Ansoldi[33,34], J. M. Antelis[35], S. Antier[36], S. Appert[1], Koya Arai[37], Koji Arai[1], Y. Arai[37], S. Araki[38], A. Araya[39], M. C. Araya[1], J. S. Areeda[25], M. Arène[36], N. Aritomi[30], N. Arnaud[40,41], S. M. Aronson[42], K. G. Arun[43], H. Asada[44], Y. Asali[45], G. Ashton[6], Y. Aso[46,47], S. M. Aston[8], P. Astone[48], F. Aubin[49], P. Aufmuth[10,11], K. AultONeal[35], C. Austin[2], S. Babak[36], F. Badaracco[18,19], M. K. M. Bader[50], S. Bae[51], Y. Bae[52], A. M. Baer[7], S. Bagnasco[53], Y. Bai[1], L. Baiotti[54], J. Baird[36], R. Bajpai[55], M. Ball[56], G. Ballardin[41], S. W. Ballmer[57], M. Bals[35], A. Balsamo[7], G. Baltus[58], S. Banagiri[59], D. Bankar[3], R. S. Bankar[3], J. C. Barayoga[1], C. Barbieri[60,61,62], B. C. Barish[1], D. Barker[63], P. Barneo[64], F. Barone[5,65], B. Barr[66], L. Barsotti[67], M. Barsuglia[36], D. Barta[68], J. Bartlett[63], M. A. Barton[23,66], I. Bartos[42], R. Bassiri[69], A. Basti[20,21], M. Bawaj[70,71], J. C. Bayley[66], A. C. Baylor[29], M. Bazzan[72,73], B. Bécsy[74], V. M. Bedakihale[75], M. Bejger[76], I. Belahcene[40], V. Benedetto[77], D. Beniwal[78], M. G. Benjamin[35], R. Benkel[79], T. F. Bennett[80], J. D. Bentley[14], M. BenYaala[32], F. Bergamin[10,11], B. K. Berger[69], S. Bernuzzi[13], C. P. L. Berry[15,66], D. Bersanetti[81], A. Bertolini[50], J. Betzwieser[8], R. Bhandare[82], A. V. Bhandari[3], D. Bhattacharjee[83], S. Bhaumik[42], J. Bidler[25], I. A. Bilenko[84], G. Billingsley[1], R. Birney[85], O. Birnholtz[86], S. Biscans[1,67], M. Bischi[87,88], S. Biscoveanu[67], A. Bisht[10,11], B. Biswas[3], M. Bitossi[20,41], M.-A. Bizouard[89], J. K. Blackburn[1], J. Blackman[90], C. D. Blair[8,91], D. G. Blair[91], R. M. Blair[63], F. Bobba[92,93], N. Bode[10,11], M. Boer[89], G. Bogaert[89], M. Boldrini[48,94], F. Bondu[95], E. Bonilla[69], R. Bonnand[49], P. Booker[10,11], B. A. Boom[50], R. Bork[1], V. Boschi[20], N. Bose[96], S. Bose[3], V. Bossilkov[91], V. Boudart[58], Y. Bouffanais[72,73], A. Bozzi[41], C. Bradaschia[20], P. R. Brady[29], A. Bramley[8], A. Branch[8], M. Branchesi[18,19], J. E. Brau[56], M. Breschi[13], T. Briant[97], J. H. Briggs[66], A. Brillet[89], M. Brinkmann[10,11], P. Brockill[29], A. F. Brooks[1], J. Brooks[41], D. D. Brown[78], S. Brunett[1], G. Bruno[98], R. Bruntz[7], J. Bryant[14], A. Buikema[67], T. Bulik[99], H. J. Bulten[50,100], A. Buonanno[79,101], R. Buscicchio[14], D. Buskulic[49], R. L. Byer[69], L. Cadonati[102], M. Caesar[103], G. Cagnoli[28], C. Cahillane[1], H. W. Cain III[2], J. Calderón Bustillo[104], J. D. Callaghan[66], T. A. Callister[105,106], E. Calloni[5,27], J. B. Camp[107], M. Canepa[81,108], M. Cannavacciuolo[92], K. C. Cannon[31], H. Cao[78], J. Cao[109], Z. Cao[110], E. Capocasa[23], E. Capote[25], G. Carapella[92,93], F. Carbognani[41], J. B. Carlin[111], M. F. Carney[15], M. Carpinelli[112,113], G. Carullo[20,21], T. L. Carver[17], J. Casanueva Diaz[41], C. Casentini[114,115], G. Castaldi[116], S. Caudill[50,117], M. Cavaglià[83], F. Cavalier[40], R. Cavalieri[41], G. Cella[20], P. Cerdá-Durán[118], E. Cesarini[115], W. Chaibi[89], K. Chakravarti[3], B. Champion[119], C.-H. Chan[120], C. Chan[31], C. L. Chan[104], M. Chan[121], K. Chandra[96], P. Chanial[41], S. Chao[120], P. Charlton[122], E. A. Chase[15], E. Chassande-Mottin[36], D. Chatterjee[29], M. Chaturvedi[82], K. Chatziioannou[1,105,106], A. Chen[104], C. Chen[123,124], H. Y. Chen[125], J. Chen[120], K. Chen[126], X. Chen[91], Y.-B. Chen[90], Y.-R. Chen[124], Z. Chen[17], H. Cheng[42], C. K. Cheong[104], H. Y. Cheung[104], H. Y. Chia[42], F. Chiadini[93,127], C-Y. Chiang[128], R. Chierici[129], A. Chincarini[81], M. L. Chiofalo[20,21], A. Chiummo[41], G. Cho[130], H. S. Cho[131], S. Choate[103], R. K. Choudhary[91], S. Choudhary[3], N. Christensen[89], H. Chu[126], Q. Chu[91], Y-K. Chu[128], S. Chua[97], K. W. Chung[132], G. Ciani[72,73], P. Ciecielag[76], M. Cieślar[76], M. Cifaldi[114,115], A. A. Ciobanu[78], R. Ciolfi[73,133], F. Cipriano[89], A. Cirone[81,108], F. Clara[63], E. N. Clark[134], J. A. Clark[102], L. Clarke[135], P. Clearwater[111], S. Clesse[136], F. Cleva[89], E. Coccia[18,19], P.-F. Cohadon[97], D. E. Cohen[40], L. Cohen[2], M. Colleoni[137], C. G. Collette[138], M. Colpi[60,61], C. M. Compton[63], M. Constancio Jr.[16], L. Conti[73], S. J. Cooper[14], P. Corban[8], T. R. Corbitt[2], I. Cordero-Carrión[139], S. Corezzi[70,71], K. R. Corley[45], N. Cornish[74], D. Corre[40], A. Corsi[140], S. Cortese[41], C. A. Costa[16], R. Cotesta[79], M. W. Coughlin[59], S. B. Coughlin[15,17], J.-P. Coulon[89], S. T. Countryman[45], B. Cousins[141], P. Couvares[1], P. B. Covas[137], D. M. Coward[91], M. J. Cowart[8], D. C. Coyne[1], R. Coyne[142], J. D. E. Creighton[29], T. D. Creighton[143], A. W. Criswell[59], M. Croquette[97], S. G. Crowder[144], J. R. Cudell[58], T. J. Cullen[2], A. Cumming[66], R. Cummings[66], E. Cuoco[20,41,145], M. Curyło[99], T. Dal Canton[40,79], G. Dálya[146], A. Dana[69], L. M. DaneshgaranBajastani[80], B. D'Angelo[81,108], S. L. Danilishin[147], S. D'Antonio[115], K. Danzmann[10,11], C. Darsow-Fromm[148], A. Dasgupta[75], L. E. H. Datrier[66], V. Dattilo[41], I. Dave[82], M. Davier[40], G. S. Davies[149,150], D. Davis[1], E. J. Daw[151], R. Dean[103], D. DeBra[69], M. Deenadayalan[3], J. Degallaix[152], M. De Laurentis[5,27], S. Deléglise[97], V. Del Favero[119], F. De Lillo[98], N. De Lillo[66], W. Del Pozzo[20,21], L. M. DeMarchi[15], F. De Matteis[114,115], V. D'Emilio[17], N. Demos[67], T. Dent[149], A. Depasse[98], R. De Pietri[153,154], R. De Rosa[5,27], C. De Rossi[41], R. DeSalvo[116], R. De Simone[127], S. Dhurandhar[3], M. C. Díaz[143], M. Diaz-Ortiz Jr.[42], N. A. Didio[57], T. Dietrich[79], L. Di Fiore[5], C. Di Fronzo[14], C. Di Giorgio[92,93], F. Di Giovanni[118], T. Di Girolamo[5,27], A. Di Lieto[20,21], B. Ding[138], S. Di Pace[48,94], I. Di Palma[48,94], F. Di Renzo[20,21], A. K. Divakarla[42], A. Dmitriev[14], Z. Doctor[56], L. D'Onofrio[5,27], F. Donovan[67], K. L. Dooley[17], S. Doravari[3], I. Dorrington[17], M. Drago[18,19], J. C. Driggers[63], Y. Drori[1], Z. Du[109], J.-G. Ducoin[40], P. Dupej[66], O. Durante[92,93], D. D'Urso[112,113], P.-A. Duverne[40], S. E. Dwyer[63], P. J. Easter[6], M. Ebersold[155], G. Eddolls[66], B. Edelman[56], T. B. Edo[1,151], O. Edy[150], A. Effler[8], S. Eguchi[121], J. Eichholz[9], S. S. Eikenberry[42], M. Eisenmann[49], R. A. Eisenstein[67], A. Ejlli[17], Y. Enomoto[30], L. Errico[5,27], R. C. Essick[125], H. Estellés[137], D. Estevez[156], Z. Etienne[157], T. Etzel[1], M. Evans[67], T. M. Evans[8], B. E. Ewing[141], V. Fafone[18,114,115], H. Fair[57], S. Fairhurst[17], X. Fan[109], A. M. Farah[125], S. Farinon[81], B. Farr[56], W. M. Farr[105,106], N. W. Farrow[6], E. J. Fauchon-Jones[17], M. Favata[158], M. Fays[58,151], M. Fazio[159], J. Feicht[1], M. M. Fejer[69], F. Feng[36], E. Fenyvesi[68,160], D. L. Ferguson[102], A. Fernandez-Galiana[67], I. Ferrante[20,21], T. A. Ferreira[16], F. Fidecaro[20,21], P. Figura[99], I. Fiori[41],

M. Fishbach[15,125], R. P. Fisher[7], R. Fittipaldi[93,161], V. Fiumara[93,162], R. Flaminio[23,49], E. Floden[59], E. Flynn[25], H. Fong[31], J. A. Font[118,163], B. Fornal[164], P. W. F. Forsyth[9], A. Franke[148], S. Frasca[48,94], F. Frasconi[20], C. Frederick[165], Z. Frei[146], A. Freise[166], R. Frey[56], P. Fritschel[67], V. V. Frolov[8], G. G. Fronzé[53], Y. Fujii[167], Y. Fujikawa[168], M. Fukunaga[37], M. Fukushima[24], P. Fulda[42], M. Fyffe[8], H. A. Gabbard[66], B. U. Gadre[79], S. M. Gaebel[14], J. R. Gair[79], J. Gais[104], S. Galaudage[6], R. Gamba[13], D. Ganapathy[67], A. Ganguly[22], D. Gao[169], S. G. Gaonkar[3], B. Garaventa[81,108], C. García-Núñez[85], C. García-Quirós[137], F. Garufi[5,27], B. Gateley[63], S. Gaudio[35], V. Gayathri[42], G. Ge[169], G. Gemme[81], A. Gennai[20], J. George[82], L. Gergely[170], P. Gewecke[148], S. Ghonge[102], Abhirup. Ghosh[79], Archisman Ghosh[171], Shaon Ghosh[29,158], Shrobana Ghosh[17], Sourath Ghosh[42], B. Giacomazzo[60,61,62], L. Giacoppo[48,94], J. A. Giaime[2,8], K. D. Giardina[8], D. R. Gibson[85], C. Gier[32], M. Giesler[90], P. Giri[20,21], F. Gissi[77], J. Glanzer[2], A. E. Gleckl[25], P. Godwin[141], E. Goetz[172], R. Goetz[42], N. Gohlke[10,11], B. Goncharov[6], G. González[2], A. Gopakumar[173], M. Gosselin[41], R. Gouaty[49], B. Grace[9], A. Grado[5,174], M. Granata[152], V. Granata[92], A. Grant[66], S. Gras[67], P. Grassia[1], C. Gray[63], R. Gray[66], G. Greco[70], A. C. Green[42], R. Green[17], A. M. Gretarsson[35], E. M. Gretarsson[35], D. Griffith[1], W. Griffiths[17], H. L. Griggs[102], G. Grignani[70,71], A. Grimaldi[175,176], E. Grimes[35], S. J. Grimm[18,19], H. Grote[17], S. Grunewald[79], P. Gruning[40], J. G. Guerrero[25], G. M. Guidi[87,88], A. R. Guimaraes[2], G. Guixé[64], H. K. Gulati[75], H.-K. Guo[164], Y. Guo[50], Anchal Gupta[1], Anuradha Gupta[177], P. Gupta[50,117], E. K. Gustafson[1], R. Gustafson[178], F. Guzman[134], S. Ha[179], L. Haegel[36], A. Hagiwara[37,180], S. Haino[128], O. Halim[34,181], E. D. Hall[67], E. Z. Hamilton[17], G. Hammond[66], W.-B. Han[182], M. Haney[155], J. Hanks[63], C. Hanna[141], M. D. Hannam[17], O. A. Hannuksela[50,104,117], H. Hansen[63], T. J. Hansen[35], J. Hanson[8], T. Harder[89], T. Hardwick[2], K. Haris[22,50,117], J. Harms[18,19], G. M. Harry[183], I. W. Harry[150], D. Hartwig[148], K. Hasegawa[37], B. Haskell[76], R. K. Hasskew[8], C.-J. Haster[67], K. Hattori[184], K. Haughian[66], H. Hayakawa[185], K. Hayama[121], F. J. Hayes[66], J. Healy[119], A. Heidmann[97], M. C. Heintze[8], J. Heinze[10,11], J. Heinzel[186], H. Heitmann[89], F. Hellman[187], P. Hello[40], A. F. Helmling-Cornell[56], G. Hemming[41], M. Hendry[66], I. S. Heng[66], E. Hennes[50], J. Hennig[10,11], M. H. Hennig[10,11], F. Hernandez Vivanco[6], M. Heurs[10,11], S. Hild[50,147], P. Hill[32], Y. Himemoto[188], T. Hinderer[189], A. S. Hines[134], Y. Hiranuma[190], N. Hirata[23], E. Hirose[37], W. C. G. Ho[191], S. Hochheim[10,11], D. Hofman[152], J. N. Hohmann[148], A. M. Holgado[26], N. A. Holland[9], I. J. Hollows[151], Z. J. Holmes[78], K. Holt[8], D. E. Holz[125], Z. Hong[192], P. Hopkins[17], J. Hough[66], E. J. Howell[91], C. G. Hoy[17], D. Hoyland[14], A. Hreibi[10,11], B-H. Hsieh[37], Y. Hsu[120], G-Z. Huang[192], H-Y. Huang[128], P. Huang[169], Y-C. Huang[124], Y.-J. Huang[128], Y.-W. Huang[67], M. T. Hübner[6], A. D. Huddart[135], E. A. Huerta[26], B. Hughey[35], D. C. Y. Hui[193], V. Hui[49], S. Husa[137], S. H. Huttner[66], R. Huxford[141], T. Huynh-Dinh[8], S. Ide[194], B. Idzkowski[99], A. Iess[114,115], B. Ikenoue[24], S. Imam[192], K. Inayoshi[195], H. Inchauspe[42], C. Ingram[78], Y. Inoue[126], G. Intini[48,94], K. Ioka[196], M. Isi[67], K. Isleif[148], K. Ito[197], Y. Itoh[198,199], B. R. Iyer[22], K. Izumi[200], V. JaberianHamedan[91], T. Jacqmin[97], S. J. Jadhav[201], S. P. Jadhav[3], A. L. James[17], A. Z. Jan[119], K. Jani[102], K. Janssens[202], N. N. Janthalur[201], P. Jaranowski[203], D. Jariwala[42], R. Jaume[137], A. C. Jenkins[132], C. Jeon[204], M. Jeunon[59], W. Jia[67], J. Jiang[42], H.-B. Jin[205,206], G. R. Johns[7], A. W. Jones[91], D. I. Jones[207], J. D. Jones[63], P. Jones[14], R. Jones[66], R. J. G. Jonker[50], L. Ju[91], K. Jung[179], P. Jung[185], J. Junker[10,11], K. Kaihotsu[197], T. Kajita[208], M. Kakizaki[184], C. V. Kalaghatgi[17], V. Kalogera[15], B. Kamai[1], M. Kamiizumi[185], N. Kanda[198,199], S. Kandhasamy[3], G. Kang[51], J. B. Kanner[1], Y. Kao[120], S. J. Kapadia[22], D. P. Kapasi[9], S. Karat[1], C. Karathanasis[209], S. Karki[83], R. Kashyap[141], M. Kasprzack[1], W. Kastaun[10,11], S. Katsanevas[41], E. Katsavounidis[67], W. Katzman[8], T. Kaur[91], K. Kawabe[63], K. Kawaguchi[37], N. Kawai[210], T. Kawasaki[30], F. Kéfélian[89], D. Keitel[137], J. S. Key[211], S. Khadka[69], F. Y. Khalili[84], I. Khan[18,115], S. Khan[17], E. A. Khazanov[212], N. Khetan[18,19], M. Khursheed[82], N. Kijbunchoo[9], C. Kim[204,213], J. C. Kim[214], J. Kim[215], K. Kim[216], W. S. Kim[52], Y.-M. Kim[179], C. Kimball[15], N. Kimura[180], P. J. King[63], M. Kinley-Hanlon[66], R. Kirchhoff[10,11], J. S. Kissel[63], N. Kita[30], H. Kitazawa[197], L. Kleybolte[148], S. Klimenko[42], A. M. Knee[172], T. D. Knowles[157], E. Knyazev[67], P. Koch[10,11], G. Koekoek[50,147], Y. Kojima[217], K. Kokeyama[185], S. Koley[50], P. Kolitsidou[17], M. Kolstein[209], K. Komori[30,67], V. Kondrashov[1], A. K. H. Kong[124], A. Kontos[218], N. Koper[10,11], M. Korobko[148], K. Kotake[121], M. Kovalam[91], D. B. Kozak[1], C. Kozakai[46], R. Kozu[219], V. Kringel[10,11], N. V. Krishnendu[10,11], A. Królak[220,221], G. Kuehn[10,11], F. Kuei[120], A. Kumar[201], P. Kumar[222], Rahul Kumar[63], Rakesh Kumar[75], J. Kume[31], K. Kuns[67], C. Kuo[126], H-S. Kuo[192], Y. Kuromiya[197], S. Kuroyanagi[223], K. Kusayanagi[210], K. Kwak[179], S. Kwang[29], D. Laghi[20,21], E. Lalande[224], T. L. Lam[104], A. Lamberts[89,225], M. Landry[63], P. Landry[25], B. B. Lane[67], R. N. Lang[67], J. Lange[119,226], B. Lantz[69], I. La Rosa[49], A. Lartaux-Vollard[40], P. D. Lasky[6], M. Laxen[8], A. Lazzarini[1], C. Lazzaro[72,73], P. Leaci[48,94], S. Leavey[10,11], Y. K. Lecoeuche[63], H. K. Lee[227], H. M. Lee[216], H. W. Lee[214], J. Lee[130], K. Lee[69], R. Lee[124], J. Lehmann[10,11], A. Lemaître[228], E. Leon[25], M. Leonardi[23], N. Leroy[40], N. Letendre[49], Y. Levin[6], J. N. Leviton[178], A. K. Y. Li[1], B. Li[120], J. Li[15], K. L. Li[124], T. G. F. Li[104], X. Li[90], C-Y. Lin[229], F-K. Lin[128], F-L. Lin[192], H. L. Lin[126], L. C.-C. Lin[179], F. Linde[50,230], S. D. Linker[80], J. N. Linley[66], T. B. Littenberg[231], G. C. Liu[123], J. Liu[10,11], K. Liu[120], X. Liu[29], M. Llorens-Monteagudo[118], R. K. L. Lo[1], A. Lockwood[232], M. L. Lollie[2], L. T. London[67], A. Longo[233,234], D. Lopez[155], M. Lorenzini[114,115], V. Loriette[235], M. Lormand[8], G. Losurdo[20], J. D. Lough[10,11], C. O. Lousto[119], G. Lovelace[25], H. Lück[10,11], D. Lumaca[114,115], A. P. Lundgren[150], L.-W. Luo[128], R. Macas[17], M. MacInnis[67], D. M. Macleod[17], I. A. O. MacMillan[1], A. Macquet[89], I. Magaña Hernandez[29], F. Magaña-Sandoval[42], C. Magazzù[20], R. M. Magee[141], R. Maggiore[14], E. Majorana[48,94], C. Makarem[1], I. Maksimovic[235], S. Maliakal[1], A. Malik[82], N. Man[89], V. Mandic[59], V. Mangano[48,94], J. L. Mango[236], G. L. Mansell[63,67], M. Manske[29], M. Mantovani[41], M. Mapelli[72,73], F. Marchesoni[70,237], M. Marchio[23], F. Marion[49], Z. Mark[90], S. Márka[45], Z. Márka[45], C. Markakis[12], A. S. Markosyan[69], A. Markowitz[1], E. Maros[1], A. Marquina[139], S. Marsat[36], F. Martelli[87,88], I. W. Martin[66], R. M. Martin[158], M. Martinez[209], V. Martinez[28], K. Martinovic[132], D. V. Martynov[14], E. J. Marx[67], H. Masalehdan[148], K. Mason[67], E. Massera[151], A. Masserot[49], T. J. Massinger[67], M. Masso-Reid[66], S. Mastrogiovanni[36], A. Matas[79], M. Mateu-Lucena[137], F. Matichard[1,67], M. Matiushechkina[10,11], N. Mavalvala[67], J. J. McCann[91], R. McCarthy[63],

D. E. McClelland[9], P. McClincy[141], S. McCormick[8], L. McCuller[67], G. I. McGhee[66], S. C. McGuire[238], C. McIsaac[150], J. McIver[172], D. J. McManus[9], T. McRae[9], S. T. McWilliams[157], D. Meacher[29], M. Mehmet[10,11], A. K. Mehta[79], A. Melatos[111], D. A. Melchor[25], G. Mendell[63], A. Menendez-Vazquez[209], C. S. Menoni[159], R. A. Mercer[29], L. Mereni[152], K. Merfeld[56], E. L. Merilh[63], J. D. Merritt[56], M. Merzougui[89], S. Meshkov[1,286], C. Messenger[66], C. Messick[226], P. M. Meyers[111], F. Meylahn[10,11], A. Mhaske[3], A. Miani[175,176], H. Miao[14], I. Michaloliakos[42], C. Michel[152], Y. Michimura[30], H. Middleton[111], L. Milano[27], A. L. Miller[42,98], M. Millhouse[111], J. C. Mills[17], E. Milotti[34,181], M. C. Milovich-Goff[80], O. Minazzoli[89,239], Y. Minenkov[115], N. Mio[240], Ll. M. Mir[209], A. Mishkin[42], C. Mishra[241], T. Mishra[42], T. Mistry[151], S. Mitra[3], V. P. Mitrofanov[84], G. Mitselmakher[42], R. Mittleman[67], O. Miyakawa[185], A. Miyamoto[198], Y. Miyazaki[30], K. Miyo[185], S. Miyoki[185], Geoffrey Mo[67], K. Mogushi[83], S. R. P. Mohapatra[67], S. R. Mohite[29], I. Molina[25], M. Molina-Ruiz[187], M. Mondin[80], M. Montani[87,88], C. J. Moore[14], D. Moraru[63], F. Morawski[76], A. More[3], C. Moreno[35], G. Moreno[63], Y. Mori[197], S. Morisaki[31,37], Y. Moriwaki[184], B. Mours[156], C. M. Mow-Lowry[14], S. Mozzon[150], F. Muciaccia[48,94], Arunava Mukherjee[66,242], D. Mukherjee[141], Soma Mukherjee[143], Subroto Mukherjee[75], N. Mukund[10,11], A. Mullavey[8], J. Munch[78], E. A. Muñiz[57], P. G. Murray[66], R. Musenich[81,108], S. L. Nadji[10,11], K. Nagano[200], S. Nagano[243], A. Nagar[53,244], K. Nakamura[23], H. Nakano[245], M. Nakano[37], R. Nakashima[210], Y. Nakayama[184], I. Nardecchia[114,115], T. Narikawa[37], L. Naticchioni[48], B. Nayak[80], R. K. Nayak[246], R. Negishi[190], B. F. Neil[91], J. Neilson[77,93], G. Nelemans[247], T. J. N. Nelson[8], M. Nery[10,11], A. Neunzert[211], K. Y. Ng[67], S. W. S. Ng[78], C. Nguyen[36], P. Nguyen[56], T. Nguyen[67], L. Nguyen Quynh[248], W.-T. Ni[169,205,249], S. A. Nichols[2], A. Nishizawa[31], S. Nissanke[50,250], F. Nocera[41], M. Noh[172], M. Norman[17], C. North[17], S. Nozaki[184], L. K. Nuttall[150], J. Oberling[63], B. D. O'Brien[42], Y. Obuchi[24], J. O'Dell[135], W. Ogaki[37], G. Oganesyan[18,19], J. J. Oh[52], K. Oh[193], S. H. Oh[52], M. Ohashi[185], N. Ohishi[46], M. Ohkawa[168], F. Ohme[10,11], H. Ohta[31], M. A. Okada[16], Y. Okutani[194], K. Okutomi[185], C. Olivetto[41], K. Oohara[190], C. Ooi[30], R. Oram[8], B. O'Reilly[8], R. G. Ormiston[59], N. D. Ormsby[7], L. F. Ortega[42], R. O'Shaughnessy[119], E. O'Shea[222], S. Oshino[185], S. Ossokine[79], C. Osthelder[1], S. Otabe[210], D. J. Ottaway[78], H. Overmier[8], A. E. Pace[141], G. Pagano[20,21], M. A. Page[91], G. Pagliaroli[18,19], A. Pai[96], S. A. Pai[82], J. R. Palamos[56], O. Palashov[212], C. Palomba[48], K. Pan[124], P. K. Panda[201], H. Pang[126], P. T. H. Pang[50,117], C. Pankow[15], F. Pannarale[48,94], B. C. Pant[82], F. Paoletti[20], A. Paoli[41], A. Paolone[48,251], A. Parisi[123], J. Park[216], W. Parker[8,238], D. Pascucci[50], A. Pasqualetti[41], R. Passaquieti[20,21], D. Passuello[20], M. Patel[7], B. Patricelli[20,41], E. Payne[6], T. C. Pechsiri[42], M. Pedraza[1], M. Pegoraro[73], A. Pele[8], F. E. Peña Arellano[185], S. Penn[252], A. Perego[175,176], A. Pereira[28], T. Pereira[253], C. J. Perez[63], C. Périgois[49], A. Perreca[175,176], S. Perriès[129], J. Petermann[148], D. Petterson[1], H. P. Pfeiffer[79], K. A. Pham[59], K. S. Phukon[3,50,230], O. J. Piccinni[48], M. Pichot[89], M. Piendibene[20,21], F. Piergiovanni[87,88], L. Pierini[48,94], V. Pierro[77,93], G. Pillant[41], F. Pilo[20], L. Pinard[152], I. M. Pinto[77,93,254,255], B. J. Piotrzkowski[29], K. Piotrzkowski[98], M. Pirello[63], M. Pitkin[256], E. Placidi[48,94], W. Plastino[233,234], C. Pluchar[134], R. Poggiani[20,21], E. Polini[49], D. Y. T. Pong[104], S. Ponrathnam[3], P. Popolizio[41], E. K. Porter[36], J. Powell[257], M. Pracchia[49], T. Pradier[156], A. K. Prajapati[75], K. Prasai[69], R. Prasanna[201], G. Pratten[14], T. Prestegard[29], M. Principe[77,93,254], G. A. Prodi[176,258], L. Prokhorov[14], P. Prosposito[114,115], L. Prudenzi[79], A. Puecher[50,117], M. Punturo[70], F. Puosi[20,21], P. Puppo[48], M. Pürrer[79], H. Qi[17], V. Quetschke[143], P. J. Quinonez[35], R. Quitzow-James[83], F. J. Raab[63], G. Raaijmakers[50,250], H. Radkins[63], N. Radulesco[89], P. Raffai[146], S. X. Rail[224], S. Raja[82], C. Rajan[82], K. E. Ramirez[143], T. D. Ramirez[25], A. Ramos-Buades[79], J. Rana[141], P. Rapagnani[48,94], U. D. Rapol[259], B. Ratto[35], A. Ray[29], V. Raymond[17], N. Raza[172], M. Razzano[20,21], J. Read[25], L. A. Rees[183], T. Regimbau[49], L. Rei[81], S. Reid[32], D. H. Reitze[1,42], P. Relton[17], P. Rettegno[53,260], F. Ricci[48,94], C. J. Richardson[35], J. W. Richardson[1], L. Richardson[134], P. M. Ricker[26], G. Riemenschneider[53,260], K. Riles[178], M. Rizzo[15], N. A. Robertson[1,66], R. Robie[1], F. Robinet[40], A. Rocchi[115], J. A. Rocha[25], S. Rodriguez[25], R. D. Rodriguez-Soto[35], L. Rolland[49], J. G. Rollins[1], V. J. Roma[56], M. Romanelli[95], R. Romano[4,5], C. L. Romel[63], A. Romero[209], I. M. Romero-Shaw[6], J. H. Romie[8], C. A. Rose[29], D. Rosińska[99], S. G. Rosofsky[26], M. P. Ross[232], S. Rowan[66], S. J. Rowlinson[14], Santosh Roy[3], Soumen Roy[261], D. Rozza[112,113], P. Ruggi[41], K. Ryan[63], S. Sachdev[141], T. Sadecki[63], J. Sadiq[149], N. Sago[262], S. Saito[24], Y. Saito[185], K. Sakai[263], Y. Sakai[190], M. Sakellariadou[132], Y. Sakuno[121], O. S. Salafia[60,61,62], L. Salconi[41], M. Saleem[43], F. Salemi[175,176], A. Samajdar[50,117], E. J. Sanchez[1], J. H. Sanchez[25], L. E. Sanchez[1], N. Sanchis-Gual[264], J. R. Sanders[265], A. Sanuy[64], T. R. Saravanan[3], N. Sarin[6], B. Sassolas[152], H. Satari[91], B. S. Sathyaprakash[17,141], S. Sato[266], T. Sato[168], O. Sauter[42,49], R. L. Savage[63], V. Savant[3], T. Sawada[198], D. Sawant[96], H. L. Sawant[3], S. Sayah[152], D. Schaetzl[1], M. Scheel[90], J. Scheuer[15], A. Schindler-Tyka[42], P. Schmidt[14], R. Schnabel[148], M. Schneewind[10,11], R. M. S. Schofield[56], A. Schönbeck[148], B. W. Schulte[10,11], B. F. Schutz[10,17], E. Schwartz[17], J. Scott[66], S. M. Scott[9], M. Seglar-Arroyo[49], E. Seidel[26], T. Sekiguchi[31], Y. Sekiguchi[267], D. Sellers[8], A. S. Sengupta[261], N. Sennett[79], D. Sentenac[41], E. G. Seo[104], V. Sequino[5,27], A. Sergeev[212], Y. Setyawati[10,11], T. Shaffer[63], M. S. Shahriar[15], B. Shams[164], L. Shao[195], S. Sharifi[2], A. Sharma[18,19], P. Sharma[82], P. Shawhan[101], N. S. Shcheblanov[228], H. Shen[26], S. Shibagaki[121], M. Shikauchi[31], R. Shimizu[24], T. Shimoda[30], K. Shimode[185], R. Shink[224], H. Shinkai[268], T. Shishido[47], A. Shoda[23], D. H. Shoemaker[67], D. M. Shoemaker[226], K. Shukla[187], S. ShyamSundar[82], M. Sieniawska[99], D. Sigg[63], L. P. Singer[107], D. Singh[141], N. Singh[99], A. Singha[50,147], A. M. Sintes[137], V. Sipala[112,113], V. Skliris[17], B. J. J. Slagmolen[9], T. J. Slaven-Blair[91], J. Smetana[14], J. R. Smith[25], R. J. E. Smith[6], S. N. Somala[269], K. Somiya[210], E. J. Son[52], K. Soni[3], S. Soni[2], B. Sorazu[66], V. Sordini[129], F. Sorrentino[81], N. Sorrentino[20,21], H. Sotani[270], R. Soulard[89], T. Souradeep[3,259], E. Sowell[140], V. Spagnuolo[50,147], A. P. Spencer[66], M. Spera[72,73], A. K. Srivastava[75], V. Srivastava[57], K. Staats[15], C. Stachie[89], D. A. Steer[36], J. Steinlechner[50,147], S. Steinlechner[50,147], D. J. Stops[14], S. Stevenson[257], M. Stover[165], K. A. Strain[66], L. C. Strang[111], G. Stratta[88,271], A. Strunk[63], R. Sturani[253], A. L. Stuver[103], J. Südbeck[148], S. Sudhagar[3], V. Sudhir[67], R. Sugimoto[200,272], H. G. Suh[29], T. Z. Summerscales[273], H. Sun[91], L. Sun[1,9], S. Sunil[75], A. Sur[76], J. Suresh[31,37], P. J. Sutton[17], Takamasa Suzuki[168],

Toshikazu Suzuki[37], B. L. Swinkels[50], M. J. Szczepańczyk[42], P. Szewczyk[99], M. Tacca[50], H. Tagoshi[37], S. C. Tait[66], H. Takahashi[274], R. Takahashi[23], A. Takamori[39], S. Takano[30], H. Takeda[30], M. Takeda[198], C. Talbot[1], H. Tanaka[275], Kazuyuki Tanaka[198], Kenta Tanaka[275], Taiki Tanaka[37], Takahiro Tanaka[262], A. J. Tanasijczuk[98], S. Tanioka[23,47], D. B. Tanner[42], D. Tao[1], A. Tapia[25], E. N. Tapia San Martin[23,50], J. D. Tasson[186], S. Telada[276], R. Tenorio[137], L. Terkowski[148], M. Test[29], M. P. Thirugnanasambandam[3], M. Thomas[8], P. Thomas[63], J. E. Thompson[17], S. R. Thondapu[82], K. A. Thorne[8], E. Thrane[6], Shubhanshu Tiwari[155], Srishti Tiwari[173], V. Tiwari[17], K. Toland[66], A. E. Tolley[150], T. Tomaru[23], Y. Tomigami[198], T. Tomura[185], M. Tonelli[20,21], A. Torres-Forné[118], C. I. Torrie[1], I. Tosta e Melo[112,113], D. Töyrä[9], A. Trapananti[70,237], F. Travasso[70,237], G. Traylor[8], M. C. Tringali[41], A. Tripathee[178], L. Troiano[93,277], A. Trovato[36], L. Trozzo[185], R. J. Trudeau[1], D. S. Tsai[120], D. Tsai[120], K. W. Tsang[50,117,278], T. Tsang[104], J-S. Tsao[192], M. Tse[67], R. Tso[90], K. Tsubono[30], S. Tsuchida[198], L. Tsukada[31], D. Tsuna[31], T. Tsutsui[31], T. Tsuzuki[24], M. Turconi[89], D. Tuyenbayev[128], A. S. Ubhi[14], N. Uchikata[37], T. Uchiyama[185], R. P. Udall[1,102], A. Ueda[180], T. Uehara[279,280], K. Ueno[31], G. Ueshima[281], D. Ugolini[282], C. S. Unnikrishnan[173], F. Uraguchi[24], A. L. Urban[2], T. Ushiba[185], S. A. Usman[125], A. C. Utina[50,147], H. Vahlbruch[10,11], G. Vajente[1], A. Vajpeyi[6], G. Valdes[2], M. Valentini[175,176], V. Valsan[29], N. van Bakel[50], M. van Beuzekom[50], J. F. J. van den Brand[50,100,147], C. Van Den Broeck[50,117], D. C. Vander-Hyde[57], L. van der Schaaf[50], J. V. van Heijningen[91,98], J. Vanosky[1], M. H. P. M. van Putten[283], M. Vardaro[50,230], A. F. Vargas[111], V. Varma[90], M. Vasúth[68], A. Vecchio[14], G. Vedovato[73], J. Veitch[66], P. J. Veitch[78], K. Venkateswara[232], J. Venneberg[10,11], G. Venugopalan[1], D. Verkindt[49], Y. Verma[82], D. Veske[45], F. Vetrano[87], A. Viceré[87,88], A. D. Viets[236], V. Villa-Ortega[149], J.-Y. Vinet[89], S. Vitale[67], T. Vo[57], H. Vocca[70,71], E. R. G. von Reis[63], J. von Wrangel[10,11], C. Vorvick[63], S. P. Vyatchanin[84], L. E. Wade[165], M. Wade[165], K. J. Wagner[119], R. C. Walet[50], M. Walker[7], G. S. Wallace[32], L. Wallace[1], S. Walsh[29], J. Wang[169], J. Z. Wang[178], W. H. Wang[143], R. L. Ward[9], J. Warner[63], M. Was[49], T. Washimi[23], N. Y. Washington[1], J. Watchi[138], B. Weaver[63], L. Wei[10,11], M. Weinert[10,11], A. J. Weinstein[1], R. Weiss[67], C. M. Weller[232], F. Wellmann[10,11], L. Wen[91], P. Weßels[10,11], J. W. Westhouse[35], K. Wette[9], J. T. Whelan[119], D. D. White[25], B. F. Whiting[42], C. Whittle[67], D. Wilken[10,11], D. Williams[66], M. J. Williams[66], A. R. Williamson[150], J. L. Willis[1], B. Willke[10,11], D. J. Wilson[134], W. Winkler[10,11], C. C. Wipf[1], T. Wlodarczyk[79], G. Woan[66], J. Woehler[10,11], J. K. Wofford[119], I. C. F. Wong[104], C. Wu[124], D. S. Wu[10,11], H. Wu[124], S. Wu[124], D. M. Wysocki[29,119], L. Xiao[1], W-R. Xu[192], T. Yamada[275], H. Yamamoto[1], Kazuhiro Yamamoto[184], Kohei Yamamoto[275], T. Yamamoto[185], K. Yamashita[184], R. Yamazaki[194], F. W. Yang[164], L. Yang[159], Yang Yang[42], Yi Yang[284], Z. Yang[59], M. J. Yap[9], D. W. Yeeles[17], A. B. Yelikar[119], M. Ying[120], K. Yokogawa[197], J. Yokoyama[30,31], T. Yokozawa[185], A. Yoon[7], T. Yoshioka[197], Hang Yu[90], Haocun Yu[67], H. Yuzurihara[37], A. Zadrożny[221], M. Zanolin[35], F. Zappa[13], S. Zeidler[285], T. Zelenova[41], J.-P. Zendri[73], M. Zevin[15], M. Zhan[169], H. Zhang[192], J. Zhang[91], L. Zhang[1], R. Zhang[42], T. Zhang[14], C. Zhao[91], G. Zhao[138], Yue Zhao[164], Yuhang Zhao[23], Z. Zhou[15], X. J. Zhu[6], Z.-H. Zhu[110], A. B. Zimmerman[226], Y. Zlochower[119], M. E. Zucker[1,67], and J. Zweizig[1]

the LIGO Scientific Collaboration, the Virgo Collaboration, and the KAGRA Collaboration

[1] LIGO Laboratory, California Institute of Technology, Pasadena, CA 91125, USA
[2] Louisiana State University, Baton Rouge, LA 70803, USA
[3] Inter-University Centre for Astronomy and Astrophysics, Pune 411007, India
[4] Dipartimento di Farmacia, Università di Salerno, I-84084 Fisciano, Salerno, Italy
[5] INFN, Sezione di Napoli, Complesso Universitario di Monte S.Angelo, I-80126 Napoli, Italy
[6] OzGrav, School of Physics & Astronomy, Monash University, Clayton 3800, VIC, Australia
[7] Christopher Newport University, Newport News, VA 23606, USA
[8] LIGO Livingston Observatory, Livingston, LA 70754, USA
[9] OzGrav, Australian National University, Canberra, ACT 0200, Australia
[10] Max Planck Institute for Gravitational Physics (Albert Einstein Institute), D-30167 Hannover, Germany
[11] Leibniz Universität Hannover, D-30167 Hannover, Germany
[12] University of Cambridge, Cambridge CB2 1TN, UK
[13] Theoretisch-Physikalisches Institut, Friedrich-Schiller-Universität Jena, D-07743 Jena, Germany
[14] University of Birmingham, Birmingham B15 2TT, UK
[15] Center for Interdisciplinary Exploration & Research in Astrophysics (CIERA), Northwestern University, Evanston, IL 60208, USA
[16] Instituto Nacional de Pesquisas Espaciais, 12227-010 São José dos Campos, São Paulo, Brazil
[17] Gravity Exploration Institute, Cardiff University, Cardiff CF24 3AA, UK
[18] Gran Sasso Science Institute (GSSI), I-67100 L'Aquila, Italy
[19] INFN, Laboratori Nazionali del Gran Sasso, I-67100 Assergi, Italy
[20] INFN, Sezione di Pisa, I-56127 Pisa, Italy
[21] Università di Pisa, I-56127 Pisa, Italy
[22] International Centre for Theoretical Sciences, Tata Institute of Fundamental Research, Bengaluru 560089, India
[23] Gravitational Wave Science Project, National Astronomical Observatory of Japan (NAOJ), Mitaka City, Tokyo 181-8588, Japan
[24] Advanced Technology Center, National Astronomical Observatory of Japan (NAOJ), Mitaka City, Tokyo 181-8588, Japan
[25] California State University Fullerton, Fullerton, CA 92831, USA
[26] NCSA, University of Illinois at Urbana-Champaign, Urbana, IL 61801, USA
[27] Università di Napoli "Federico II," Complesso Universitario di Monte S.Angelo, I-80126 Napoli, Italy
[28] Université de Lyon, Université Claude Bernard Lyon 1, CNRS, Institut Lumière Matière, F-69622 Villeurbanne, France
[29] University of Wisconsin–Milwaukee, Milwaukee, WI 53201, USA
[30] Department of Physics, The University of Tokyo, Bunkyo-ku, Tokyo 113-0033, Japan
[31] Research Center for the Early Universe (RESCEU), The University of Tokyo, Bunkyo-ku, Tokyo 113-0033, Japan
[32] SUPA, University of Strathclyde, Glasgow G1 1XQ, UK
[33] Dipartimento di Matematica e Informatica, Università di Udine, I-33100 Udine, Italy
[34] INFN, Sezione di Trieste, I-34127 Trieste, Italy
[35] Embry-Riddle Aeronautical University, Prescott, AZ 86301, USA

[36] Université de Paris, CNRS, Astroparticule et Cosmologie, F-75006 Paris, France
[37] Institute for Cosmic Ray Research (ICRR), KAGRA Observatory, The University of Tokyo, Kashiwa City, Chiba 277-8582, Japan
[38] Accelerator Laboratory, High Energy Accelerator Research Organization (KEK), Tsukuba City, Ibaraki 305-0801, Japan
[39] Earthquake Research Institute, The University of Tokyo, Bunkyo-ku, Tokyo 113-0032, Japan
[40] Université Paris-Saclay, CNRS/IN2P3, IJCLab, F-91405 Orsay, France
[41] European Gravitational Observatory (EGO), I-56021 Cascina, Pisa, Italy
[42] University of Florida, Gainesville, FL 32611, USA
[43] Chennai Mathematical Institute, Chennai 603103, India
[44] Department of Mathematics and Physics, Hirosaki University, Hirosaki City, Aomori 036-8561, Japan
[45] Columbia University, New York, NY 10027, USA
[46] Kamioka Branch, National Astronomical Observatory of Japan (NAOJ), Kamioka-cho, Hida City, Gifu 506-1205, Japan
[47] The Graduate University for Advanced Studies (SOKENDAI), Mitaka City, Tokyo 181-8588, Japan
[48] INFN, Sezione di Roma, I-00185 Roma, Italy
[49] Univ. Grenoble Alpes, Laboratoire d'Annecy de Physique des Particules (LAPP), Université Savoie Mont Blanc, CNRS/IN2P3, F-74941 Annecy, France
[50] Nikhef, Science Park 105, 1098 XG Amsterdam, Netherlands
[51] Korea Institute of Science and Technology Information (KISTI), Yuseong-gu, Daejeon 34141, Republic of Korea
[52] National Institute for Mathematical Sciences, Daejeon 34047, Republic of Korea
[53] INFN Sezione di Torino, I-10125 Torino, Italy
[54] International College, Osaka University, Toyonaka City, Osaka 560-0043, Japan
[55] School of High Energy Accelerator Science, The Graduate University for Advanced Studies (SOKENDAI), Tsukuba City, Ibaraki 305-0801, Japan
[56] University of Oregon, Eugene, OR 97403, USA
[57] Syracuse University, Syracuse, NY 13244, USA
[58] Université de Liège, B-4000 Liège, Belgium
[59] University of Minnesota, Minneapolis, MN 55455, USA
[60] Università degli Studi di Milano-Bicocca, I-20126 Milano, Italy
[61] INFN, Sezione di Milano-Bicocca, I-20126 Milano, Italy
[62] INAF, Osservatorio Astronomico di Brera sede di Merate, I-23807 Merate, Lecco, Italy
[63] LIGO Hanford Observatory, Richland, WA 99352, USA
[64] Institut de Ciències del Cosmos, Universitat de Barcelona, C/Martí i Franquès 1, Barcelona, E-08028, Spain
[65] Dipartimento di Medicina, Chirurgia e Odontoiatria "Scuola Medica Salernitana," Università di Salerno, I-84081 Baronissi, Salerno, Italy
[66] SUPA, University of Glasgow, Glasgow G12 8QQ, UK
[67] LIGO Laboratory, Massachusetts Institute of Technology, Cambridge, MA 02139, USA
[68] Wigner RCP, RMKI, H-1121 Budapest, Konkoly Thege Miklós út 29-33, Hungary
[69] Stanford University, Stanford, CA 94305, USA
[70] INFN, Sezione di Perugia, I-06123 Perugia, Italy
[71] Università di Perugia, I-06123 Perugia, Italy
[72] Università di Padova, Dipartimento di Fisica e Astronomia, I-35131 Padova, Italy
[73] INFN, Sezione di Padova, I-35131 Padova, Italy
[74] Montana State University, Bozeman, MT 59717, USA
[75] Institute for Plasma Research, Bhat, Gandhinagar 382428, India
[76] Nicolaus Copernicus Astronomical Center, Polish Academy of Sciences, 00-716, Warsaw, Poland
[77] Dipartimento di Ingegneria, Università del Sannio, I-82100 Benevento, Italy
[78] OzGrav, University of Adelaide, Adelaide, SA 5005, Australia
[79] Max Planck Institute for Gravitational Physics (Albert Einstein Institute), D-14476 Potsdam, Germany
[80] California State University, Los Angeles, 5151 State University Dr., Los Angeles, CA 90032, USA
[81] INFN, Sezione di Genova, I-16146 Genova, Italy
[82] RRCAT, Indore, Madhya Pradesh 452013, India
[83] Missouri University of Science and Technology, Rolla, MO 65409, USA
[84] Faculty of Physics, Lomonosov Moscow State University, Moscow 119991, Russia
[85] SUPA, University of the West of Scotland, Paisley PA1 2BE, UK
[86] Bar-Ilan University, Ramat Gan, 5290002, Israel
[87] Università degli Studi di Urbino "Carlo Bo," I-61029 Urbino, Italy
[88] INFN, Sezione di Firenze, I-50019 Sesto Fiorentino, Firenze, Italy
[89] Artemis, Université Côte d'Azur, Observatoire de la Côte d'Azur, CNRS, F-06304 Nice, France
[90] CaRT, California Institute of Technology, Pasadena, CA 91125, USA
[91] OzGrav, University of Western Australia, Crawley, WA 6009, Australia
[92] Dipartimento di Fisica "E.R. Caianiello," Università di Salerno, I-84084 Fisciano, Salerno, Italy
[93] INFN, Sezione di Napoli, Gruppo Collegato di Salerno, Complesso Universitario di Monte S. Angelo, I-80126 Napoli, Italy
[94] Università di Roma "La Sapienza," I-00185 Roma, Italy
[95] Univ Rennes, CNRS, Institut FOTON - UMR6082, F-3500 Rennes, France
[96] Indian Institute of Technology Bombay, Powai, Mumbai 400 076, India
[97] Laboratoire Kastler Brossel, Sorbonne Université, CNRS, ENS-Université PSL, Collège de France, F-75005 Paris, France
[98] Université catholique de Louvain, B-1348 Louvain-la-Neuve, Belgium
[99] Astronomical Observatory Warsaw University, 00-478 Warsaw, Poland
[100] VU University Amsterdam, 1081 HV Amsterdam, Netherlands
[101] University of Maryland, College Park, MD 20742, USA
[102] School of Physics, Georgia Institute of Technology, Atlanta, GA 30332, USA
[103] Villanova University, 800 Lancaster Ave., Villanova, PA 19085, USA
[104] Faculty of Science, Department of Physics, The Chinese University of Hong Kong, Shatin, N.T., Hong Kong
[105] Stony Brook University, Stony Brook, NY 11794, USA
[106] Center for Computational Astrophysics, Flatiron Institute, New York, NY 10010, USA
[107] NASA Goddard Space Flight Center, Greenbelt, MD 20771, USA
[108] Dipartimento di Fisica, Università degli Studi di Genova, I-16146 Genova, Italy
[109] Tsinghua University, Beijing 100084, People's Republic of China

[110] Department of Astronomy, Beijing Normal University, Beijing 100875, People's Republic of China
[111] OzGrav, University of Melbourne, Parkville, VIC 3010, Australia
[112] Università degli Studi di Sassari, I-07100 Sassari, Italy
[113] INFN, Laboratori Nazionali del Sud, I-95125 Catania, Italy
[114] Università di Roma Tor Vergata, I-00133 Roma, Italy
[115] INFN, Sezione di Roma Tor Vergata, I-00133 Roma, Italy
[116] University of Sannio at Benevento, I-82100 Benevento, Italy and INFN, Sezione di Napoli, I-80100 Napoli, Italy
[117] Institute for Gravitational and Subatomic Physics (GRASP), Utrecht University, Princetonplein 1, 3584 CC Utrecht, Netherlands
[118] Departamento de Astronomía y Astrofísica, Universitat de València, E-46100 Burjassot, València, Spain
[119] Rochester Institute of Technology, Rochester, NY 14623, USA
[120] National Tsing Hua University, Hsinchu City, 30013 Taiwan, Republic of China
[121] Department of Applied Physics, Fukuoka University, Jonan, Fukuoka City, Fukuoka 814-0180, Japan
[122] OzGrav, Charles Sturt University, Wagga Wagga, NSW 2678, Australia
[123] Department of Physics, Tamkang University, Danshui Dist., New Taipei City 25137, Taiwan
[124] Department of Physics and Institute of Astronomy, National Tsing Hua University, Hsinchu 30013, Taiwan
[125] University of Chicago, Chicago, IL 60637, USA
[126] Department of Physics, Center for High Energy and High Field Physics, National Central University, Zhongli District, Taoyuan City 32001, Taiwan
[127] Dipartimento di Ingegneria Industriale (DIIN), Università di Salerno, I-84084 Fisciano, Salerno, Italy
[128] Institute of Physics, Academia Sinica, Nankang, Taipei 11529, Taiwan
[129] Institut de Physique des 2 Infinis de Lyon (IP2I), CNRS/IN2P3, Université de Lyon, Université Claude Bernard Lyon 1, F-69622 Villeurbanne, France
[130] Seoul National University, Seoul 08826, Republic of Korea
[131] Pusan National University, Busan 46241, Republic of Korea
[132] King's College London, University of London, London WC2R 2LS, UK
[133] INAF, Osservatorio Astronomico di Padova, I-35122 Padova, Italy
[134] University of Arizona, Tucson, AZ 85721, USA
[135] Rutherford Appleton Laboratory, Didcot OX11 0DE, UK
[136] Université libre de Bruxelles, Avenue Franklin Roosevelt B-50-1050 Bruxelles, Belgium
[137] Universitat de les Illes Balears, IAC3—IEEC, E-07122 Palma de Mallorca, Spain
[138] Université Libre de Bruxelles, Brussels B-1050, Belgium
[139] Departamento de Matemáticas, Universitat de València, E-46100 Burjassot, València, Spain
[140] Texas Tech University, Lubbock, TX 79409, USA
[141] The Pennsylvania State University, University Park, PA 16802, USA
[142] University of Rhode Island, Kingston, RI 02881, USA
[143] The University of Texas Rio Grande Valley, Brownsville, TX 78520, USA
[144] Bellevue College, Bellevue, WA 98007, USA
[145] Scuola Normale Superiore, Piazza dei Cavalieri, I-7-56126 Pisa, Italy
[146] MTA-ELTE Astrophysics Research Group, Institute of Physics, Eötvös University, Budapest 1117, Hungary
[147] Maastricht University, 6200 MD, Maastricht, Netherlands
[148] Universität Hamburg, D-22761 Hamburg, Germany
[149] IGFAE, Campus Sur, Universidade de Santiago de Compostela, E-15782, Spain
[150] University of Portsmouth, Portsmouth, PO1 3FX, UK
[151] The University of Sheffield, Sheffield S10 2TN, UK
[152] Laboratoire des Matériaux Avancés (LMA), Institut de Physique des 2 Infinis (IP2I) de Lyon, CNRS/IN2P3, Université de Lyon, Université Claude Bernard Lyon 1, F-69622 Villeurbanne, France
[153] Dipartimento di Scienze Matematiche, Fisiche e Informatiche, Università di Parma, I-43124 Parma, Italy
[154] INFN, Sezione di Milano Bicocca, Gruppo Collegato di Parma, I-43124 Parma, Italy
[155] Physik-Institut, University of Zurich, Winterthurerstrasse 190, 8057 Zurich, Switzerland
[156] Université de Strasbourg, CNRS, IPHC UMR 7178, F-67000 Strasbourg, France
[157] West Virginia University, Morgantown, WV 26506, USA
[158] Montclair State University, Montclair, NJ 07043, USA
[159] Colorado State University, Fort Collins, CO 80523, USA
[160] Institute for Nuclear Research, Hungarian Academy of Sciences, Bem t'er 18/c, H-4026 Debrecen, Hungary
[161] CNR-SPIN, c/o Università di Salerno, I-84084 Fisciano, Salerno, Italy
[162] Scuola di Ingegneria, Università della Basilicata, I-85100 Potenza, Italy
[163] Observatori Astronòmic, Universitat de València, E-46980 Paterna, València, Spain
[164] The University of Utah, Salt Lake City, UT 84112, USA
[165] Kenyon College, Gambier, OH 43022, USA
[166] Vrije Universiteit Amsterdam, 1081 HV, Amsterdam, Netherlands
[167] Department of Astronomy, The University of Tokyo, Mitaka City, Tokyo 181-8588, Japan
[168] Faculty of Engineering, Niigata University, Nishi-ku, Niigata City, Niigata 950-2181, Japan
[169] State Key Laboratory of Magnetic Resonance and Atomic and Molecular Physics, Innovation Academy for Precision Measurement Science and Technology (APM), Chinese Academy of Sciences, Xiao Hong Shan, Wuhan 430071, People's Republic of China
[170] University of Szeged, Dóm tér 9, Szeged 6720, Hungary
[171] Universiteit Gent, B-9000 Gent, Belgium
[172] University of British Columbia, Vancouver, BC V6T 1Z4, Canada
[173] Tata Institute of Fundamental Research, Mumbai 400005, India
[174] INAF, Osservatorio Astronomico di Capodimonte, I-80131 Napoli, Italy
[175] Università di Trento, Dipartimento di Fisica, I-38123 Povo, Trento, Italy
[176] INFN, Trento Institute for Fundamental Physics and Applications, I-38123 Povo, Trento, Italy
[177] University of Mississippi, University, MS 38677, USA
[178] University of Michigan, Ann Arbor, MI 48109, USA
[179] Department of Physics, School of Natural Science, Ulsan National Institute of Science and Technology (UNIST), Ulju-gun, Ulsan 44919, Republic of Korea
[180] Applied Research Laboratory, High Energy Accelerator Research Organization (KEK), Tsukuba City, Ibaraki 305-0801, Japan
[181] Dipartimento di Fisica, Università di Trieste, I-34127 Trieste, Italy
[182] Shanghai Astronomical Observatory, Chinese Academy of Sciences, Shanghai 200030, People's Republic of China
[183] American University, Washington, DC 20016, USA

[184] Faculty of Science, University of Toyama, Toyama City, Toyama 930-8555, Japan
[185] Institute for Cosmic Ray Research (ICRR), KAGRA Observatory, The University of Tokyo, Kamioka-cho, Hida City, Gifu 506-1205, Japan
[186] Carleton College, Northfield, MN 55057, USA
[187] University of California, Berkeley, CA 94720, USA
[188] College of Industrial Technology, Nihon University, Narashino City, Chiba 275-8575, Japan
[189] Institute for Theoretical Physics (ITP), Utrecht University, Princetonplein 5, 3584 CC Utrecht, Netherlands
[190] Graduate School of Science and Technology, Niigata University, Nishi-ku, Niigata City, Niigata 950-2181, Japan
[191] Department of Physics and Astronomy, Haverford College, Haverford, PA 19041, USA
[192] Department of Physics, National Taiwan Normal University, Sec. 4, Taipei 116, Taiwan
[193] Astronomy & Space Science, Chungnam National University, Yuseong-gu, Daejeon 34134, Republic of Korea
[194] Department of Physics and Mathematics, Aoyama Gakuin University, Sagamihara City, Kanagawa 252-5258, Japan
[195] Kavli Institute for Astronomy and Astrophysics, Peking University, Haidian District, Beijing 100871, People's Republic of China
[196] Yukawa Institute for Theoretical Physics (YITP), Kyoto University, Sakyou-ku, Kyoto City, Kyoto 606-8502, Japan
[197] Graduate School of Science and Engineering, University of Toyama, Toyama City, Toyama 930-8555, Japan
[198] Department of Physics, Graduate School of Science, Osaka City University, Sumiyoshi-ku, Osaka City, Osaka 558-8585, Japan
[199] Nambu Yoichiro Institute of Theoretical and Experimental Physics (NITEP), Osaka City University, Sumiyoshi-ku, Osaka City, Osaka 558-8585, Japan
[200] Institute of Space and Astronautical Science (JAXA), Chuo-ku, Sagamihara City, Kanagawa 252-0222, Japan
[201] Directorate of Construction, Services & Estate Management, Mumbai 400094, India
[202] Universiteit Antwerpen, Prinsstraat 13, B-2000 Antwerpen, Belgium
[203] University of Białystok, 15-424 Białystok, Poland
[204] Department of Physics, Ewha Womans University, Seodaemun-gu, Seoul 03760, Republic of Korea
[205] National Astronomical Observatories, Chinese Academic of Sciences, Chaoyang District, Beijing, People's Republic of China
[206] School of Astronomy and Space Science, University of Chinese Academy of Sciences, Chaoyang District, Beijing, People's Republic of China
[207] University of Southampton, Southampton SO17 1BJ, UK
[208] Institute for Cosmic Ray Research (ICRR), The University of Tokyo, Kashiwa City, Chiba 277-8582, Japan
[209] Institut de Física d'Altes Energies (IFAE), Barcelona Institute of Science and Technology, and ICREA, E-08193 Barcelona, Spain
[210] Graduate School of Science and Technology, Tokyo Institute of Technology, Meguro-ku, Tokyo 152-8551, Japan
[211] University of Washington Bothell, Bothell, WA 98011, USA
[212] Institute of Applied Physics, Nizhny Novgorod, 603950, Russia
[213] Ewha Womans University, Seoul 03760, Republic of Korea
[214] Inje University Gimhae, South Gyeongsang 50834, Republic of Korea
[215] Department of Physics, Myongji University, Yongin 17058, Republic of Korea
[216] Korea Astronomy and Space Science Institute (KASI), Yuseong-gu, Daejeon 34055, Republic of Korea
[217] Department of Physical Science, Hiroshima University, Higashihiroshima City, Hiroshima 903-0213, Japan
[218] Bard College, 30 Campus Rd., Annandale-on-Hudson, NY 12504, USA
[219] Institute for Cosmic Ray Research (ICRR), Research Center for Cosmic Neutrinos (RCCN), The University of Tokyo, Kamioka-cho, Hida City, Gifu 506-1205, Japan
[220] Institute of Mathematics, Polish Academy of Sciences, 00656 Warsaw, Poland
[221] National Center for Nuclear Research, 05-400 Świerk-Otwock, Poland
[222] Cornell University, Ithaca, NY 14850, USA
[223] Institute for Advanced Research, Nagoya University, Furocho, Chikusa-ku, Nagoya City, Aichi 464-8602, Japan
[224] Université de Montréal/Polytechnique, Montreal, QC H3T 1J4, Canada
[225] Laboratoire Lagrange, Université Côte d'Azur, Observatoire Côte d'Azur, CNRS, F-06304 Nice, France
[226] Department of Physics, University of Texas, Austin, TX 78712, USA
[227] Department of Physics, Hanyang University, Seoul 04763, Republic of Korea
[228] NAVIER, École des Ponts, Univ. Gustave Eiffel, CNRS, Marne-la-Vallée, France
[229] National Center for High-Performance Computing, National Applied Research Laboratories, Hsinchu Science Park, Hsinchu City 30076, Taiwan
[230] Institute for High-Energy Physics, University of Amsterdam, Science Park 904, 1098 XH Amsterdam, Netherlands
[231] NASA Marshall Space Flight Center, Huntsville, AL 35811, USA
[232] University of Washington, Seattle, WA 98195, USA
[233] Dipartimento di Matematica e Fisica, Università degli Studi Roma Tre, I-00146 Roma, Italy
[234] INFN, Sezione di Roma Tre, I-00146 Roma, Italy
[235] ESPCI, CNRS, F-75005 Paris, France
[236] Concordia University Wisconsin, Mequon, WI 53097, USA
[237] Università di Camerino, Dipartimento di Fisica, I-62032 Camerino, Italy
[238] Southern University and A&M College, Baton Rouge, LA 70813, USA
[239] Centre Scientifique de Monaco, 8 quai Antoine Ier, MC-98000, Monaco
[240] Institute for Photon Science and Technology, The University of Tokyo, Bunkyo-ku, Tokyo 113-8656, Japan
[241] Indian Institute of Technology Madras, Chennai 600036, India
[242] Saha Institute of Nuclear Physics, Bidhannagar, West Bengal 700064, India
[243] The Applied Electromagnetic Research Institute, National Institute of Information and Communications Technology (NICT), Koganei City, Tokyo 184-8795, Japan
[244] Institut des Hautes Etudes Scientifiques, F-91440 Bures-sur-Yvette, France
[245] Faculty of Law, Ryukoku University, Fushimi-ku, Kyoto City, Kyoto 612-8577, Japan
[246] Indian Institute of Science Education and Research, Kolkata, Mohanpur, West Bengal 741252, India
[247] Department of Astrophysics/IMAPP, Radboud University Nijmegen, P.O. Box 9010, 6500 GL Nijmegen, Netherlands
[248] Department of Physics, University of Notre Dame, Notre Dame, IN 46556, USA
[249] Department of Physics, National Tsing Hua University, Hsinchu 30013, Taiwan
[250] GRAPPA, Anton Pannekoek Institute for Astronomy and Institute for High-Energy Physics, University of Amsterdam, Science Park 904, 1098 XH Amsterdam, Netherlands
[251] Consiglio Nazionale delle Ricerche—Istituto dei Sistemi Complessi, Piazzale Aldo Moro 5, I-00185 Roma, Italy
[252] Hobart and William Smith Colleges, Geneva, NY 14456, USA
[253] International Institute of Physics, Universidade Federal do Rio Grande do Norte, Natal RN 59078-970, Brazil
[254] Museo Storico della Fisica e Centro Studi e Ricerche "Enrico Fermi," I-00184 Roma, Italy
[255] Department of Engineering, University of Sannio, Benevento I-82100, Italy
[256] Lancaster University, Lancaster LA1 4YW, UK

[257] OzGrav, Swinburne University of Technology, Hawthorn VIC 3122, Australia
[258] Università di Trento, Dipartimento di Matematica, I-38123 Povo, Trento, Italy
[259] Indian Institute of Science Education and Research, Pune, Maharashtra 411008, India
[260] Dipartimento di Fisica, Università degli Studi di Torino, I-10125 Torino, Italy
[261] Indian Institute of Technology, Palaj, Gandhinagar, Gujarat 382355, India
[262] Department of Physics, Kyoto University, Sakyou-ku, Kyoto City, Kyoto 606-8502, Japan
[263] Department of Electronic Control Engineering, National Institute of Technology, Nagaoka College, Nagaoka City, Niigata 940-8532, Japan
[264] Centro de Astrofísica e Gravitação (CENTRA), Departamento de Física, Instituto Superior Técnico, Universidade de Lisboa, 1049-001 Lisboa, Portugal
[265] Marquette University, 11420 W. Clybourn St., Milwaukee, WI 53233, USA
[266] Graduate School of Science and Engineering, Hosei University, Koganei City, Tokyo 184-8584, Japan
[267] Faculty of Science, Toho University, Funabashi City, Chiba 274-8510, Japan
[268] Faculty of Information Science and Technology, Osaka Institute of Technology, Hirakata City, Osaka 573-0196, Japan
[269] Indian Institute of Technology Hyderabad, Sangareddy, Khandi, Telangana 502285, India
[270] iTHEMS (Interdisciplinary Theoretical and Mathematical Sciences Program), The Institute of Physical and Chemical Research (RIKEN), Wako, Saitama 351-0198, Japan
[271] INAF, Osservatorio di Astrofisica e Scienza dello Spazio, I-40129 Bologna, Italy
[272] Department of Space and Astronautical Science, The Graduate University for Advanced Studies (SOKENDAI), Sagamihara, Kanagawa 252-5210, Japan
[273] Andrews University, Berrien Springs, MI 49104, USA
[274] Research Center for Space Science, Advanced Research Laboratories, Tokyo City University, Setagaya, Tokyo 158-0082, Japan
[275] Institute for Cosmic Ray Research (ICRR), Research Center for Cosmic Neutrinos (RCCN), The University of Tokyo, Kashiwa City, Chiba 277-8582, Japan
[276] National Metrology Institute of Japan, National Institute of Advanced Industrial Science and Technology, Tsukuba City, Ibaraki 305-8568, Japan
[277] Dipartimento di Scienze Aziendali - Management and Innovation Systems (DISA-MIS), Università di Salerno, I-84084 Fisciano, Salerno, Italy
[278] Van Swinderen Institute for Particle Physics and Gravity, University of Groningen, Nijenborgh 4, 9747 AG Groningen, Netherlands
[279] Department of Communications Engineering, National Defense Academy of Japan, Yokosuka City, Kanagawa 239-8686, Japan
[280] Department of Physics, University of Florida, Gainesville, FL 32611, USA
[281] Department of Information and Management Systems Engineering, Nagaoka University of Technology, Nagaoka City, Niigata 940-2188, Japan
[282] Trinity University, San Antonio, TX 78212, USA
[283] Department of Physics and Astronomy, Sejong University, Gwangjin-gu, Seoul 143-747, Republic of Korea
[284] Department of Electrophysics, National Chiao Tung University, Hsinchu, Taiwan
[285] Department of Physics, Rikkyo University, Toshima-ku, Tokyo 171-8501, Japan
Received 2021 April 29; revised 2021 June 3; accepted 2021 June 4; published 2021 June 29

Abstract

We report the observation of gravitational waves from two compact binary coalescences in LIGO's and Virgo's third observing run with properties consistent with neutron star–black hole (NSBH) binaries. The two events are named GW200105_162426 and GW200115_042309, abbreviated as GW200105 and GW200115; the first was observed by LIGO Livingston and Virgo and the second by all three LIGO–Virgo detectors. The source of GW200105 has component masses $8.9^{+1.2}_{-1.5}$ and $1.9^{+0.3}_{-0.2}\,M_{\odot}$, whereas the source of GW200115 has component masses $5.7^{+1.8}_{-2.1}$ and $1.5^{+0.7}_{-0.3}\,M_{\odot}$ (all measurements quoted at the 90% credible level). The probability that the secondary's mass is below the maximal mass of a neutron star is 89%–96% and 87%–98%, respectively, for GW200105 and GW200115, with the ranges arising from different astrophysical assumptions. The source luminosity distances are 280^{+110}_{-110} and 300^{+150}_{-100} Mpc, respectively. The magnitude of the primary spin of GW200105 is less than 0.23 at the 90% credible level, and its orientation is unconstrained. For GW200115, the primary spin has a negative spin projection onto the orbital angular momentum at 88% probability. We are unable to constrain the spin or tidal deformation of the secondary component for either event. We infer an NSBH merger rate density of 45^{+75}_{-33} Gpc^{-3} yr^{-1} when assuming that GW200105 and GW200115 are representative of the NSBH population or 130^{+112}_{-69} Gpc^{-3} yr^{-1} under the assumption of a broader distribution of component masses.

1. Introduction

In 2020 January, the LIGO–Virgo detector network observed gravitational-wave (GW) signals from two compact binary inspirals that are consistent with neutron star–black hole (NSBH) binaries. These represent the first confident observations to date of NSBH binaries via any observational means. The two events, carrying the full designations GW200105_162426 and GW200115_042309 and abbreviated henceforth as GW200105 and GW200115, were detected on 2020 January 5 at 16:24:26 UTC and 2020 January 15 at 04:23:10 UTC, respectively. The coincident detection of GW200115 by the three detectors LIGO Hanford, LIGO Livingston, and Virgo gives it high confidence of being an astrophysical GW event. During the other event, GW200105, the LIGO Hanford detector was not operational, and, owing to the small signal-to-noise ratio (S/N) in Virgo, it was effectively a single-detector event in LIGO Livingston. While quantification of the confidence of single-detector events is subject to significant uncertainty, GW200105 stands clearly apart in the LIGO Livingston data from any other candidate with NSBH-like parameters during the ∼11 months of the third observing run (O3).

The component masses inferred from these binary inspirals provide information on the nature of their components. The primaries have masses of $m_1 = 8.9^{+1.2}_{-1.5}$ and $5.7^{+1.8}_{-2.1}\,M_{\odot}$ for GW200105 and GW200115, respectively, with uncertainties quoted at the 90% credible level. These primary masses are well above the maximum mass of a neutron star (NS; Rhoades & Ruffini 1974; Abbott et al. 2018a; Cromartie et al. 2019; Shibata et al. 2019; Farr & Chatziioannou 2020; Fonseca et al. 2021; Nathanail et al. 2021) and within the mass range of black holes (BHs) observed electromagnetically (Özel et al. 2010;

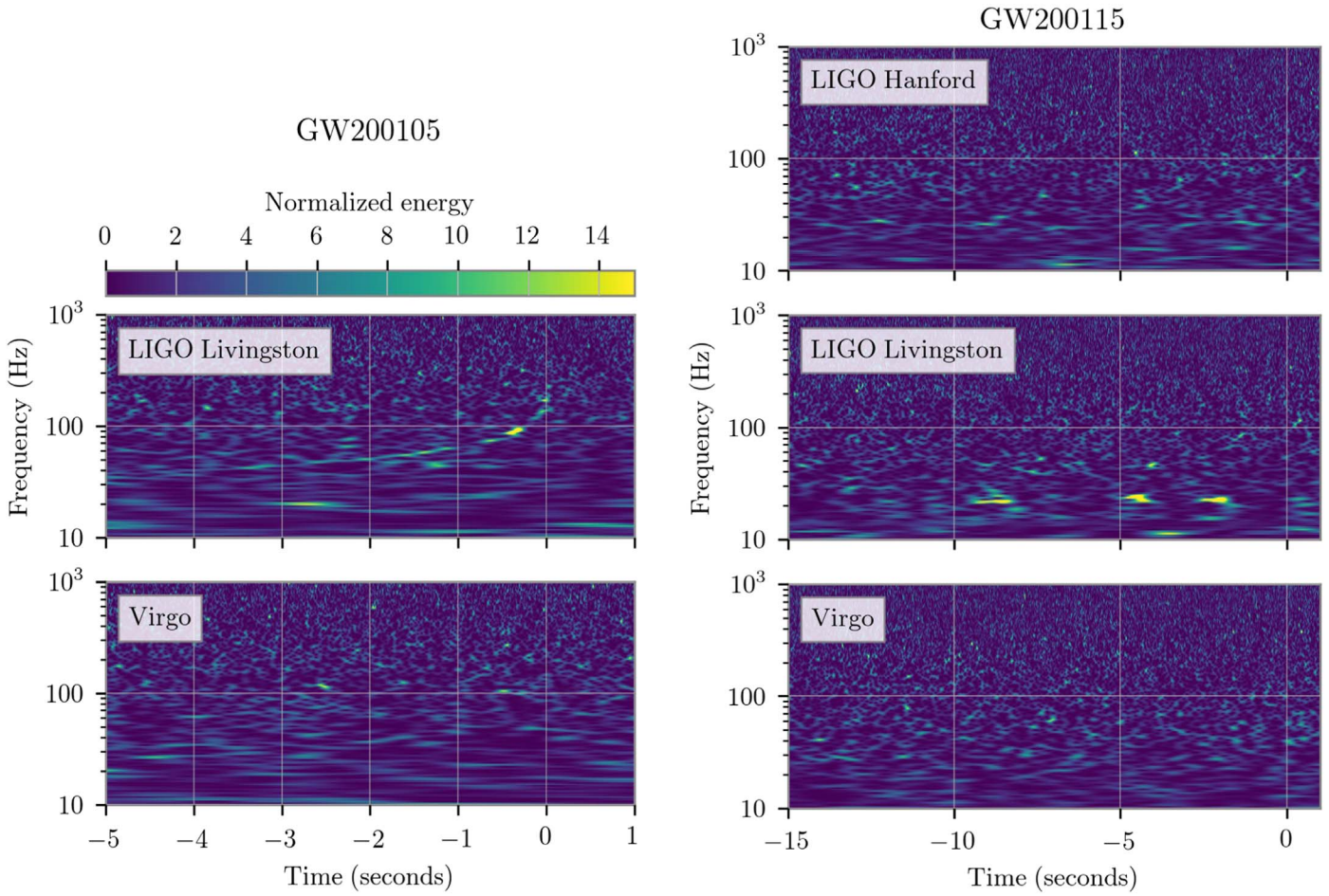

Figure 1. Time–frequency representations of the data containing GW200105 (left column) and GW200115 (right column). Times are shown relative to the signals' merger times, 2020 January 5 at 16:24:26 UTC (left) and 2020 January 15 at 04:23:10 UTC (right). The amplitude scale of each time–frequency tile is normalized by the respective detector's noise amplitude spectral density. The LIGO Livingston data of GW200105 show a track of excess power with increasing frequency. In the other panels, no similar tracks are visible, as the S/N in each of the detectors is lower and (for GW200115) the signal is longer. For GW200105, the LIGO Livingston data are shown after glitch subtraction. For GW200115, light-scattering noise is visible in LIGO Livingston below 25 Hz.

Farr et al. 2011; Kreidberg et al. 2012; Miller & Miller 2014) and via GWs (Abbott et al. 2016a, 2019c, 2021b). The masses of the secondaries are $m_2 = 1.9^{+0.3}_{-0.2}$ and $1.5^{+0.7}_{-0.3}\,M_\odot$, respectively, for GW200105 and GW200115, within the mass range of known NSs (Antoniadis et al. 2016; Abbott et al. 2017a, 2020a; Alsing et al. 2018).

Detections of NSBHs have so far remained elusive in both electromagnetic (EM) and GW surveys. In the past four decades, surveys have identified 19 binary neutron star (BNS) systems in the Galaxy (Farrow et al. 2019; Agazie et al. 2021); however, the discovery of a pulsar in an NSBH binary remains a key objective for current and future radio observations (Liu et al. 2014; Weltman et al. 2020).

Similarly, GW observations of LIGO and Virgo through the first part of the O3 run (O3a) have led to the identification of 48 binary black hole (BBH) candidates (Abbott et al. 2019c, 2021b) and two BNS candidates (Abbott et al. 2017a, 2020d). Independent analyses of the public detector data identified additional GW candidates (Magee et al. 2019; Nitz et al. 2019b, 2020a, 2021; Venumadhav et al. 2019, 2020; Zackay et al. 2019a, 2019b). The absence of NSBH candidates in LIGO's and Virgo's first and second observing runs (O1 and O2, respectively) led to the upper limit on the local merger rate density of NSBH systems of $\mathcal{R}_{\rm NSBH} \leqslant 610\ {\rm Gpc}^{-3}\,{\rm yr}^{-1}$ at the 90% credible level (Abbott et al. 2019c).

During O3a, two events were notable as possible NSBH candidates. First, GW190426_152155 (Abbott et al. 2021b) was identified as a marginal NSBH candidate with a false-alarm rate (FAR; $1.4\ {\rm yr}^{-1}$) so high that it could also plausibly be a detector noise artifact. Second, GW190814 (Abbott et al. 2020c) may have been an NSBH merger. Although GW190814's secondary mass of $m_2 = 2.59^{+0.08}_{-0.09}\,M_\odot$ likely exceeds the maximum mass supported by slowly spinning NSs (Essick & Landry 2020; Fattoyev et al. 2020; Godzieba et al. 2021; Tews et al. 2021), such as those found in known binaries that will coalesce within a Hubble time, the secondary could conceivably be an NS spinning near its breakup frequency (Essick & Landry 2020; Most et al. 2020; Dexheimer et al. 2021; Tews et al. 2021).

The existence of NSBH systems has long been conjectured. Observations in the Milky Way reveal high-mass X-ray binaries composed of a massive star and a compact object (Liu et al. 2008; Gou et al. 2009, 2014; Orosz et al. 2009, 2011). Binary evolution models show that X-ray binaries with a BH component are possible progenitors of NSBH systems (Belczynski et al. 2013; Grudzinska et al. 2015).

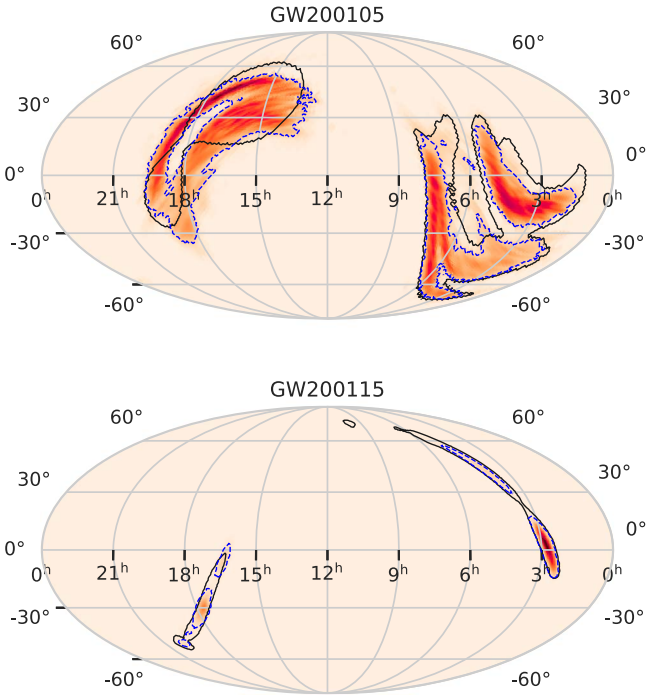

Figure 2. Sky localizations for GW200105 (top) and GW200115 (bottom) in terms of R.A. and decl. The thick solid contours show the 90% credible regions from the low-latency sky localization algorithm BAYESTAR (Singer & Price 2016). The shaded patch is the sky map obtained from the preferred high-spin analysis of Section 4, with the 90% credible regions bounded by the thin dotted contours.

Major uncertainties regarding massive binary evolution, such as mass loss, mass transfer, and the impact of supernova explosions result in a wide range of merger rate predictions: 0.1–800 $\mathrm{Gpc}^{-3}\,\mathrm{yr}^{-1}$ (Belczynski et al. 2002, 2006, 2016; Sipior & Sigurdsson 2002; Dominik et al. 2015; Eldridge et al. 2017; Kruckow et al. 2018; Mapelli & Giacobbo 2018; Neijssel et al. 2019; Drozda et al. 2020; Zevin et al. 2020; Broekgaarden et al. 2021). Comparable NSBH merger rates are predicted from young star clusters (Ziosi et al. 2014; Rastello et al. 2020), while NSBH merger rates in globular and nuclear clusters are predicted to be orders of magnitude lower (Clausen et al. 2013; Arca Sedda 2020; Fragione & Banerjee 2020; Hoang et al. 2020; Ye et al. 2020). Measuring the NSBH merger rate and properties such as masses and spins is crucial in determining formation channels.

This Letter presents the status of the detectors during times around GW200105 and GW200115 (Section 2) and the results of the different searches leading to the detections (Section 3). We describe the main properties of the two events (Section 4) and discuss the nature of the secondary components (Section 5). Finally, we present the astrophysical implications, including the merger rates of this new class of GW source (Section 6), and conclude (Section 7). Data products associated with the events reported here, such as calibrated strain time series and parameter estimation posterior samples, are available through the Gravitational Wave Open Science Center (GWOSC) at gw-openscience.org.

2. Detectors and Data

The two events reported here were observed in the second part of the third observing run (O3b). At the time of GW200105, LIGO Livingston had been in a stable operational state for over 10 hr, with a sensitivity, quantified by the angle-averaged BNS inspiral range (Allen et al. 2012), of ∼137 Mpc. Virgo had been in its nominal state for ∼22 hr with a BNS range of ∼45 Mpc, and LIGO Hanford was not operational. At the time of GW200115, all three interferometers had been in a stable operational state for over 2 hr. The BNS ranges for LIGO Hanford, LIGO Livingston, and Virgo around the detection were ∼115, ∼133, and ∼50 Mpc, respectively.

Figure 1 shows time–frequency representations (Chatterji et al. 2004) of the two events. The LIGO Livingston data of GW200105 show a track of excess power with increasing frequency. For GW200115, no similar tracks are visible, as the S/N in each of the detectors is lower than that of GW200105 in LIGO Livingston (see Figure 3). Also, light-scattering noise (Soni et al. 2020, 2021) is visible in Figure 1 in LIGO Livingston around 20 Hz.

The LIGO and Virgo GW detectors are calibrated using radiation pressure from auxiliary lasers at a known frequency and amplitude (Acernese et al. 2018; Sun et al. 2020). In LIGO, the calibration pipeline (Viets et al. 2018) linearly subtracts the noise from the calibration lines and the harmonics of the power mains from the data.

The calibration systematic error and associated uncertainty of the data in the [20–1024] Hz frequency region are for the LIGO detectors no larger than 8.6% in amplitude and 5.9° in phase for GW200105 and 8.0% in amplitude and 5.5° in phase for GW200115 (68% credible intervals). For Virgo, we use 5.0% in amplitude and 4.1° in phase for both events, except for frequencies 46–51 Hz, where additional calibration systematic error arises from online loops set up to damp the main power lines at 50 Hz and mechanical resonances of the suspensions close to 48 Hz. This effect was introduced during detector improvements carried out between O3a and O3b and is not accounted for in the signal reconstruction process. However, Virgo data in the frequency window 46–51 Hz are excluded from the parameter estimation analyses in Section 4.

To verify that instrumental noise artifacts do not bias the analysis of source properties of the observed events, we use data quality validation procedures as in previous events (Abbott et al. 2016e; Davis et al. 2021), employing sensor arrays at LIGO and Virgo to measure environmental disturbances that could couple into the interferometers (Nguyen et al. 2021). In Virgo, we find no evidence of excess power from terrestrial sources for both events. For GW200105, we identify light-scattering noise in LIGO Livingston below 25 Hz, 3 s before merger. As in past detections (Abbott et al. 2021b), we subtract this noise with the BayesWave algorithm (Cornish et al. 2021) and use the cleaned data for the source parameter estimation in Section 4. The top left panel of Figure 1 shows the cleaned data. A low-energy feature around 20 Hz, not overlapping with the time–frequency track of GW200105, remains after the glitch subtraction. For GW200115, we also identify light scattering in the LIGO Livingston data below 25 Hz. Due to the increased difficulty of subtracting the long-duration glitching that coincides with the time–frequency track of GW200115, glitch-subtracted data were not available at the time of analysis. Hence, we exclude LIGO Livingston data below 25 Hz in the analysis in Section 4.

Table 1
Network S/N Recovered by the Search Pipelines in Low Latency and Later Offline Analysis with Improved Calibration and Refined Data Quality Information

Event		GSTLAL	MBTA	PYCBC	SPIIR
GW200105	Low latency	13.9	13.3	13.2*	13.2
	Offline	13.9	13.4	13.1*	⋯
GW200115	Low latency	11.4	11.4	11.3	11.0
	Offline	11.6	11.2	10.8*	⋯

Note. An asterisk indicates values where Virgo is not included in the S/N calculation.

3. Detections

Event GW200115 is a coincident event, and in Section 3.1, we describe the established procedures to identify it and determine its significance. Subsequently, we describe the procedures followed for the single-detector event GW200105.

3.1. GW200115—Multi-detector Event

Event GW200115 was initially identified by all four low-latency matched-filtering pipelines as a possible compact binary coalescence (CBC) candidate in LIGO Hanford and LIGO Livingston: GSTLAL (Cannon et al. 2012; Privitera et al. 2014; Messick et al. 2017; Sachdev et al. 2019; Hanna et al. 2020), MBTA ONLINE (Adams et al. 2016; Aubin et al. 2021), PYCBC LIVE (Usman et al. 2016; Nitz et al. 2017, 2018, 2019a; Dal Canton et al. 2020), and SPIIR (Hooper et al. 2012; Luan et al. 2012; Guo et al. 2018; Chu et al. 2020). As detailed in Abbott et al. (2021b), matched-filtering searches use banks (Owen & Sathyaprakash 1999; Harry et al. 2009; Privitera et al. 2014; Roy et al. 2017, 2019) of modeled gravitational waveforms with the mass range relevant to GW200105 and GW200115 covered by the SEOBNRv4_ROM waveform model (Pürrer 2016; Bohé et al. 2017). The signal in Virgo was not loud enough to further improve the significance of the coincident candidate observed by the LIGO detectors, so GW200115 was reported as a two-detector event in the GRACEDB event database named S200115j with a merger time of 2020 January 15 at 04:23:10 UTC.

A public Preliminary Gamma-ray burst Coordinates Network (GCN) Notice was sent out 6 minutes after the event (LIGO Scientific Collaboration & Virgo Collaboration 2020a). The low-latency BAYESTAR (Singer & Price 2016) sky map computed from the original trigger, which was produced from MBTA ONLINE, indicated a possible discrepancy compared to those from the other three pipelines. Therefore, the representative trigger was manually switched to the one from GSTLAL (LIGO Scientific Collaboration & Virgo Collaboration 2020b). The associated sky map is shown in the bottom panel of Figure 2 with a solid black line with 90% credible area of 900 deg^2. The GCN Circular reported a probability >99% for the lighter compact object to have a mass below 3 $M_\odot$, derived from a machine-learning analysis (Chatterjee et al. 2020; Kapadia et al. 2020). The RAVEN pipeline (Urban 2016), which looks for coincident gamma-ray bursts (GRBs), did not report an associated GRB trigger from Fermi-GBM or the Neil Gehrels Swift Observatory within −1 and +5 s of the GW trigger. A total of 31 GCN Circulars (GCN archive for S200115j; 2020) reporting follow-up observations were published for this event. To date, no EM counterpart has been reported associated with GW200115.

After the low-latency identification of GW200115, the extended periods of strain data around the event are further analyzed by the detection pipelines in their offline configurations using improved calibration and refined data quality information that is not available in low latency (Abbott et al. 2018b, 2021b; Davis et al. 2021). In this analysis, we also subtract nonstationary noise due to the nonlinear coupling of the 60 Hz power mains at the LIGO detectors using coupling functions derived from machine-learning techniques (Vajente et al. 2020).

The PYCBC uses a template bank constructed with a hybrid geometric-random algorithm (Roy et al. 2017, 2019), while GSTLAL and MBTA use a template bank generated by a stochastic placement method (Babak 2008; Privitera et al. 2014; Mukherjee et al. 2021). The GSTLAL identifies GW200115 with a network S/N of 11.6 and FAR of $<1/(1\times10^5\,\mathrm{yr})$ using the data from 2019 November 1 15:00 UTC to 2020 January 22 18:11 UTC. The MBTA and PYCBC offline analyses also identified the trigger in data from 2020 January 13 10:27 UTC to 2020 January 22 18:11 UTC, yielding consistent network S/Ns as shown in Table 1, as well as estimated FARs of $1/(182\,\mathrm{yr})$ and $<1/(5.6\times10^4\,\mathrm{yr})$, respectively. Based on two detectors, these FARs robustly indicate the confidence of the detection.

3.2. GW200105—Single-detector Event

Event GW200105 was identified by GSTLAL running in the low-latency configuration as a possible CBC candidate in LIGO Livingston and Virgo data with a network S/N of 13.9 and merger time 2020 January 5 at 16:24:26 UTC. The candidate identified as S200105ae in GRACEDB was considered a single-detector event because the S/N in Virgo was below the threshold S/N of 4.0.

The low-latency FAR of ≈24/yr did not pass the threshold for sending a GCN alert. Without the information provided by temporal coincidence between different detectors and consistency in recovered parameters, it is more difficult to obtain a robust estimate of the event's significance. In fact, an alternative configuration of GSTLAL, running to test several improvements made in the offline configuration of early O3 (Abbott et al. 2021b), found the trigger at higher significance. Therefore, validation procedures and subsequent early-offline analysis were initiated. The three other low-latency search pipelines, MBTA ONLINE, PYCBC LIVE, and SPIIR, also generated triggers with consistent S/Ns near the event time of S200105ae (see Table 1). These three pipelines were not configured to assign FARs to single-detector triggers and therefore did not generate automatic alerts for GW200105.

On 2020 January 6 at 19:39:09 UTC, the initial GCN Circular reported a low-latency BAYESTAR skymap (solid black contours) in the top panel of Figure 2 with 90% credible region of 7700 deg^2 and a 12% chance of formation of tidally disrupted matter—relevant for a possible EM counterpart—as a result of the coalescence, as derived from a machine-learning analysis (Chatterjee et al. 2020; Kapadia et al. 2020). Using the parameters obtained from low-latency parameter estimation, the chance of formation of tidally disrupted material was later revised to be negligible (see LIGO Scientific Collaboration & Virgo Collaboration 2020c and Section 5 below).

In response to the discovery notice of GW200105, multiple observatories carried out follow-up and shared their results publicly

via 21 GCN circulars (GCN archive for S200105ae 2020). To date, no EM counterpart has been reported associated with GW200105.

After the event's identification in low latency, the strain data are further analyzed by the detection pipelines in their offline configuration, following procedures for single-detector events discussed in Abbott et al. (2020a). Here GSTLAL identifies GW200105 with an S/N of 13.9 and FAR of 1/(2.8 yr) in its offline configuration using data from 2019 November 1 15:00 UTC up to 2020 January 22 18:11 UTC. For single-detector events, like GW200105, the FAR estimate involves extrapolation, as explained below. The MBTA and PYCBC offline analyses also identify the trigger in the LIGO Livingston data from 2020 January 4 17:09 UTC to 2020 January 13 10:27 UTC yielding the consistent S/Ns shown in Table 1. The S/N for GW200105 is larger than that for GW200115, even though LIGO Hanford was not operational.

We cannot rely on only the S/N of the CBC trigger to estimate its significance, i.e., to quantify how often detector noise mimics a possible coalescence signal. Because detector noise shows significant deviation in the tails from the standard Gaussianity assumptions, its properties have to be estimated empirically (Abbott et al. 2016b). For multi-detector triggers like GW200115, consistency of the observed CBC trigger among two or more detectors forms an integral part of establishing it as a confident detection with a low FAR. On the other hand, single-detector triggers can be assigned only modest FAR values due to limited detector observational time (Callister et al. 2017; Nitz et al. 2020b). Nonetheless, alternative methods can be used to estimate confidence in a single-detector event, as was demonstrated for GW190425 (Abbott et al. 2020a).

The signal GW200105 measured in LIGO Livingston is distinct from all noise events in the entire O3 observation period. Specifically, Figure 3 shows with colored shading the distribution of background noise triggers identified by GSTLAL in the region of binary systems with a chirp mass less than 4 $M_{\odot}$. The colored region indicates the density of background noise triggers quantified through the S/N–ξ^2 noise probability density function for the three detectors, where the autocorrelation ξ^2 provides a consistency test similar to χ^2 (Messick et al. 2017). The red star represents GW200105, which lies in a region of this plane without noise triggers, indicating that this trigger is unique within the entire O3.

For comparison, Figure 3 also shows GW200115 and the marginal candidate GW190426_152155 separately for LIGO Livingston and LIGO Hanford. In general, triggers such as GW200115 and GW190426_152155 in Figure 3 would not be separable from the noise by a single detector alone, and it is the coincidence between multiple detectors that raises their significance. On the other hand, the coincidence was not available for GW200105, yet it clearly stands out from the background in Figure 3, as strong GW signals typically do.

The uniqueness of GW200105 within the data shown leads to a upper bound on the FAR assignment comparable to the inverse observing time. A stronger bound, like the FAR quoted above, must rely on assumptions made on the properties of the noise triggers if one had collected the observational strain data for a longer period, a process called extrapolation. As a consequence of the assumptions made, the extrapolated FAR estimates have large uncertainties. Since single-detector FAR estimates rely on the uniqueness within the data set, the values may change and errors may reduce as more data are accumulated. At the time of the analysis, neither MBTA nor PYCBC had the capability to assign a significance to single-detector triggers, although GW200105 also stands out as a unique trigger in their analyses. Based on these considerations, we consider this trigger to be astrophysical and include it in the analysis in the remainder of this paper.

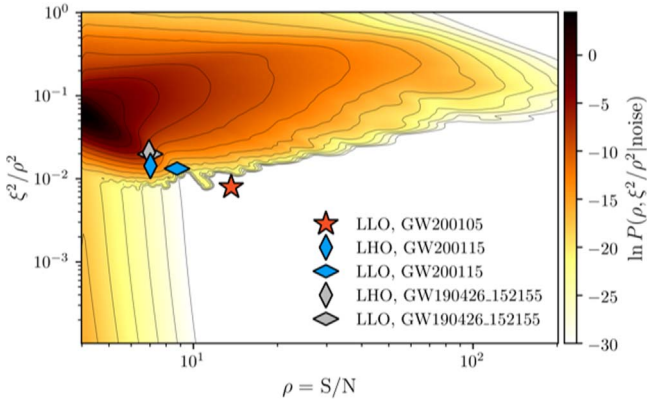

Figure 3. Colored shading shows the joint S/N–ξ^2 noise probability density function for LIGO Hanford (LHO), LIGO Livingston (LLO), and Virgo, computed from background triggers found by GSTLAL in the region of lighter binary systems during the entire O3. The red star indicates GW200105. At its position, there is no background present, indicating that it stands above all of the recorded background triggers. For comparison, the triggers of GW200115 and the marginal GW190426_152155 are also shown.

4. Source Properties

We infer the physical properties of the two GW events using a coherent Bayesian analysis following the methodology described in Appendix B of Abbott et al. (2019c). For GW200105, data from LIGO Livingston and Virgo are analyzed, whereas for GW200115, data from both LIGO detectors and Virgo are used.

Owing to the different signal durations, we analyze 32 s of data for the higher-mass event GW200105 and 64 s of data for GW200115. All likelihood evaluations use a low-frequency cutoff of $f_{\mathrm{low}} = 20$ Hz, except for LIGO Livingston for GW200115, where $f_{\mathrm{low}} = 25$ Hz avoids excess noise localized at low frequencies, as discussed in Section 2. The power spectral density used in the likelihood calculations is the median estimate calculated with BayesLine (Cornish & Littenberg 2015).

The parallel Bilby (PBILBY) inference library, together with the DYNESTY nested sampling software (Ashton et al. 2019; Romero-Shaw et al. 2020b; Smith et al. 2020; Speagle 2020), is the primary tool used to sample the posterior distribution of the sources' parameters and perform hypothesis testing. In addition, we use RIFT (Lange et al. 2018) for the most computationally expensive analyses and LALINFERENCE (Veitch et al. 2015) for verification.

We base our main analyses of GW200105 and GW200115 on BBH waveform models that include the effects of spin-induced orbital precession and higher-order multipole GW moments but do not include tidal effects on the secondary. Specifically, we use two signal models: IMRPhenomXPHM (Phenom PHM; Pratten et al. 2020a) from the phenomenological family and SEOBNRv4PHM (EOBNR PHM; Ossokine et al. 2020) from the effective one-body numerical relativity family. The acronym PHM stands for Precessing Higher-order

Table 2
Source Properties of GW200105 and GW200115

	GW200105		GW200115	
	Low Spin ($\chi_2 < 0.05$)	High Spin ($\chi_2 < 0.99$)	Low Spin ($\chi_2 < 0.05$)	High Spin ($\chi_2 < 0.99$)
Primary mass $m_1/M_\odot$	$8.9^{+1.1}_{-1.3}$	$8.9^{+1.2}_{-1.5}$	$5.9^{+1.4}_{-2.1}$	$5.7^{+1.8}_{-2.1}$
Secondary mass $m_2/M_\odot$	$1.9^{+0.2}_{-0.2}$	$1.9^{+0.3}_{-0.2}$	$1.4^{+0.6}_{-0.2}$	$1.5^{+0.7}_{-0.3}$
Mass ratio q	$0.21^{+0.06}_{-0.04}$	$0.22^{+0.08}_{-0.04}$	$0.24^{+0.31}_{-0.08}$	$0.26^{+0.35}_{-0.10}$
Total mass $M/M_\odot$	$10.8^{+0.9}_{-1.0}$	$10.9^{+1.1}_{-1.2}$	$7.3^{+1.2}_{-1.5}$	$7.1^{+1.5}_{-1.4}$
Chirp mass $\mathcal{M}/M_\odot$	$3.41^{+0.08}_{-0.07}$	$3.41^{+0.08}_{-0.07}$	$2.42^{+0.05}_{-0.07}$	$2.42^{+0.05}_{-0.07}$
Detector-frame chirp mass $(1+z)\mathcal{M}/M_\odot$	$3.619^{+0.006}_{-0.006}$	$3.619^{+0.007}_{-0.008}$	$2.580^{+0.006}_{-0.007}$	$2.579^{+0.007}_{-0.007}$
Primary spin magnitude χ_1	$0.09^{+0.18}_{-0.08}$	$0.08^{+0.22}_{-0.08}$	$0.31^{+0.52}_{-0.29}$	$0.33^{+0.48}_{-0.29}$
Effective inspiral spin parameter $\chi_{\rm eff}$	$-0.01^{+0.08}_{-0.12}$	$-0.01^{+0.11}_{-0.15}$	$-0.14^{+0.17}_{-0.34}$	$-0.19^{+0.23}_{-0.35}$
Effective precession spin parameter χ_p	$0.07^{+0.15}_{-0.06}$	$0.09^{+0.14}_{-0.07}$	$0.19^{+0.28}_{-0.17}$	$0.21^{+0.30}_{-0.17}$
Luminosity distance $D_{\rm L}$/Mpc	280^{+110}_{-110}	280^{+110}_{-110}	310^{+150}_{-110}	300^{+150}_{-100}
Source redshift z	$0.06^{+0.02}_{-0.02}$	$0.06^{+0.02}_{-0.02}$	$0.07^{+0.03}_{-0.02}$	$0.07^{+0.03}_{-0.02}$

Note. We report the median values with 90% credible intervals. Parameter estimates are obtained using the Combined PHM samples.

multipole Moments. Henceforth, we will use the shortened names for the waveform models.

In order to quantify the impact of neglecting tidal effects, we also analyze GW200105 and GW200115 using two NSBH waveform models that include tidal effects and assume that spins are aligned with the orbital angular momentum: IMRPhenomNSBH (Phenom NSBH; Thompson et al. 2020) and SEOBNRv4_ROM_NRTidalv2_NSBH (EOBNR NSBH; Matas et al. 2020). We restrict the NSBH analyses to the region of applicability of the NSBH models, i.e., $\chi_1 < 0.5$, $\chi_2 < 0.05$ for Phenom NSBH and $\chi_1 < 0.9$, $\chi_2 < 0.05$ for EOBNR NSBH. We also perform aligned-spin BBH waveform analyses and find good agreement with the analyses using NSBH waveform models (see Section 4.6 below), validating the use of BBH waveform models. Specifically, we use the aligned-spin BBH models IMRPhenomXAS (Phenom; Pratten et al. 2020b) and SEOBNRv4 (EOBNR; Bohé et al. 2017), which only contain dominant quadrupole moments, and IMRPhenomXHM (Phenom HM; García-Quirós et al. 2020) and SEOBNRv4HM (EOBNR HM; Cotesta et al. 2018, 2020), which contain higher-order moments.

The secondary objects are probably NSs based on mass estimates, as discussed in detail in Section 5. As in earlier GW analyses (Abbott et al. 2017a, 2020b), we proceed with two different priors on the secondary's spin magnitude: a low-spin prior, $\chi_2 \leqslant 0.05$, which captures the maximum spin observed in Galactic BNSs that will merge within a Hubble time (Burgay et al. 2003), and a high-spin prior, $\chi_2 \leqslant 0.99$, which is agnostic about the nature of the compact object. The two priors allow us to investigate whether the astrophysically relevant subcase of low NS spin leads to differences in the parameter estimation for the binaries. All other priors are set as in previous analyses (e.g., Abbott et al. 2021b). Throughout, we assume a standard flat ΛCDM cosmology with Hubble constant $H_0 = 67.9\,{\rm km\,s^{-1}\,Mpc^{-1}}$ and matter density parameter $\Omega_{\rm m} = 0.3065$ (Ade et al. 2016).

For each spin prior, we run our main analyses with higher-order multipole moments and precession for both waveform families, EOBNR PHM and Phenom PHM. The EOBNR PHM model is used in combination with RIFT and the Phenom PHM model with PBILBY. The parameter estimation results for the individual precessing waveform models yield results in very good agreement; the median values typically differ by 1/10 of the width of the 90% credible interval. Nevertheless, in order to alleviate potential biases due to different samplers or waveform models, we combine an equal number of samples of each into one data set for each spin prior (Abbott et al. 2016c, 2020c; Ashton & Khan 2020) and denote these as Combined PHM. The quoted parameter estimates in the following sections are the Combined PHM high-spin prior analyses. In the figures, we emphasize the high-spin prior results. The values of the most important parameters of the binaries are summarized in

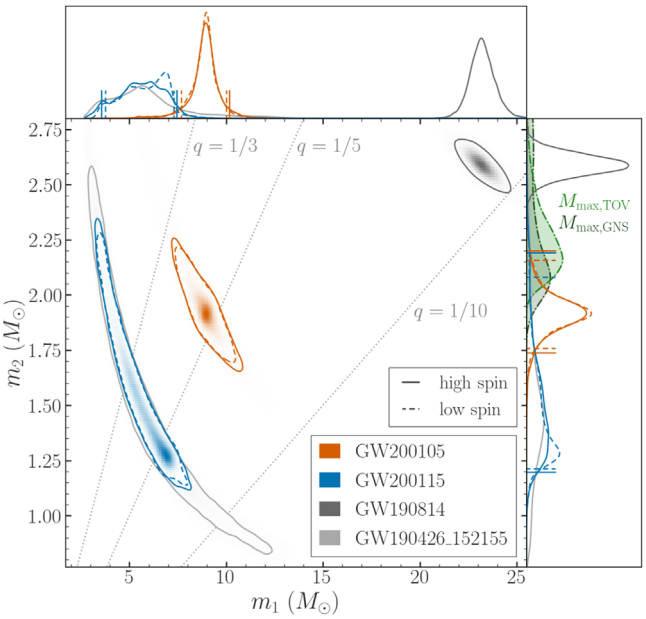

Figure 4. Component masses of GW200105 (red) and GW200115 (blue), represented by their two- and one-dimensional posterior distributions. Colored shading and solid curves indicate the high-spin prior, whereas dashed curves represent the low-spin prior. The contours in the main panel, as well as the vertical and horizontal lines in the top and right panels, respectively, indicate the 90% credible intervals. Also shown in gray are two possible NSBH events, GW190814 and the marginal candidate GW190426_152155, the latter overlapping GW200115. Lines of constant mass ratio are indicated in dashed gray. The green shaded curves in the right panel represent the one-dimensional probability densities for two estimates of the maximum NS mass, based on analyses of nonrotating NSs ($M_{\rm max,TOV}$; Landry et al. 2020, 2021) and Galactic NSs ($M_{\rm max,GNS}$; Farr & Chatziioannou 2020).

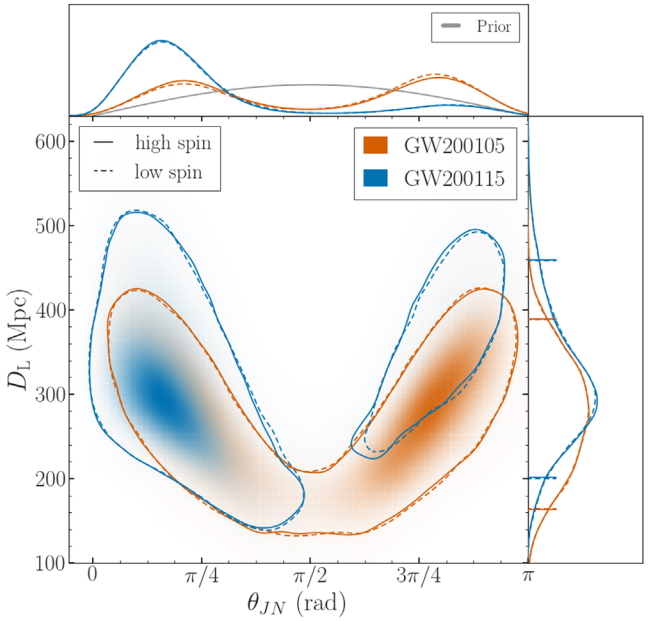

Figure 5. Two- and one-dimensional posterior distributions for distance D_L and inclination θ_{JN}. The solid (dashed) lines indicate the high-spin (low-spin) prior analysis, and the shading indicates the posterior probability of the high-spin prior analysis. The contours in the main panel and the horizontal lines in the right panel indicate 90% credible intervals.

Table 2, and we will present the details in the following sections.

4.1. Masses

Figure 4 shows the posterior distribution for the component masses of the two binaries. Defining the mass parameters such that the heavier mass is the primary object, i.e., $m_1 > m_2$, our analysis shows that GW200105 is a binary with a mass ratio of $q = m_2/m_1 = 0.22^{+0.08}_{-0.04}$, with source component masses $m_1 = 8.9^{+1.2}_{-1.5}$ and $m_2 = 1.9^{+0.3}_{-0.2}\,M_\odot$. Similarly, GW200115 is a binary with a mass ratio of $q = 0.26^{+0.35}_{-0.10}$, with source component masses $m_1 = 5.7^{+1.8}_{-2.1}$ and $m_2 = 1.5^{+0.7}_{-0.3}\,M_\odot$.

The primary components of GW200105 and GW200115 are identified as BHs from their mass measurements. For GW200115, we find that the probability of the primary falling in the lower mass gap ($3\,M_\odot \lesssim m_1 \lesssim 5\,M_\odot$; Bailyn et al. 1998; Orosz et al. 1998) is 30% (27%) for a high-spin (low-spin) prior. For context, Figure 4 also includes two potential NSBH candidates discovered previously; GW190814 (Abbott et al. 2020c) is a high-S/N event with well-measured masses that has a significantly more massive primary and a distinctly more massive secondary than either GW200105 or GW200115, and the marginal candidate GW190426_152155 (Abbott et al. 2021b) has (if of astrophysical origin) m_1–m_2 contours that overlap those of GW200115. The masses of GW190426_152155 are less constrained than those of GW200115 due to its smaller S/N. To highlight how the secondary masses of GW200105 and GW200115 compare to the maximum NS mass, we also show two estimates of the maximum NS mass based on analyses of nonrotating (Landry et al. 2020) and Galactic (Farr & Chatziioannou 2020) NSs.

The secondary masses are consistent with the maximum NS mass, which we quantify in Section 5.2.

4.2. Sky Location, Distance, and Inclination

We localize GW200105's source to a sky area of 7200 deg^2 (90% credible region). The large sky area arises due to the absence of data from LIGO Hanford. The luminosity distance of the source is found to be $D_L = 280^{+110}_{-110}$ Mpc. For the second event, GW200115, we localize its source to be within 600 deg^2. It is better localized than GW200105 by an order of magnitude, since GW200115 was observed with three detectors. We find the luminosity distance of the source to be $D_L = 300^{+150}_{-100}$ Mpc.

The luminosity distance is degenerate with the inclination angle θ_{JN} between the line of sight and the binaries' total angular momentum vector (Cutler & Flanagan 1994; Nissanke et al. 2010). Inclination $\theta_{JN} = 0$ indicates that the angular momentum vector points toward Earth. The posterior distribution of the inclination angle is bimodal and strongly correlated with luminosity distance, as shown in Figure 5. The inclination measurement for GW200105 equally favors orbits that are either oriented toward or away from the line of sight. In contrast, GW200115 shows modest preference for an orientation $\theta_{JN} \leqslant \pi/2$.

4.3. Spins

The angular momentum vector $\boldsymbol{S}_i$ of each compact object is related to its dimensionless spin vector $\boldsymbol{\chi}_i \equiv c\boldsymbol{S}_i/(Gm_i^2)$. Its magnitude $\chi_i \equiv |\boldsymbol{\chi}_i|$ is bounded by 1. For GW200105, we infer $\chi_1 = 0.08^{+0.22}_{-0.08}$, which is consistent with zero. For GW200115, the spin magnitude is not as tightly constrained, $\chi_1 = 0.33^{+0.48}_{-0.29}$, but is also consistent with zero. The spin of the secondary for both events is unconstrained.

One of the best-constrained spin parameters is the effective inspiral spin parameter $\chi_{\rm eff}$ (Damour 2001; Racine 2008; Santamaría et al. 2010; Ajith et al. 2014; Vitale et al. 2017b). It encodes information about the binaries' spin components parallel to the orbital angular momentum, $\chi_{\rm eff} = \left(\frac{m_1}{M}\boldsymbol{\chi}_1 + \frac{m_2}{M}\boldsymbol{\chi}_2\right)\cdot\hat{L}$, where $\hat{L}$ is the unit vector along the orbital angular momentum.

For GW200105, $\chi_{\rm eff} = -0.01^{+0.11}_{-0.15}$, and we find the effective inspiral spin parameter to be strongly peaked about zero, with roughly equal support for being either positive or negative. For GW200115, we find modest support for negative effective inspiral spin: $\chi_{\rm eff} = -0.19^{+0.23}_{-0.35}$. Negative values of $\chi_{\rm eff}$ indicate binaries with at least one spin component negatively aligned with respect to the orbital angular momentum, i.e., $\chi_{i,z} \equiv \boldsymbol{\chi}_i \cdot \hat{L} < 0$. We find $\chi_{1,z} = -0.19^{+0.24}_{-0.50}$ and a probability of 88% that $\chi_{1,z} < 0$.

The joint posterior probability of the dimensionless spin angular momentum magnitude and tilt angle for both components of both events is shown in Figure 6. The tilt angle with respect to the orbital angular momentum is defined as $\arccos(\hat{L}.\hat{\chi}_i)$. Deviations from uniform shading indicate a spin orientation measurement. The spin orientation of the primary of GW200105 is unconstrained, whereas the orientation of GW200115 shows support for negatively aligned primary spin.

Orbital precession is caused by a spin component in the orbital plane of a binary (Apostolatos et al. 1994), which we parameterize using the effective precession spin parameter $0 \leqslant \chi_{\rm p} \leqslant 1$ (Schmidt et al. 2015). We infer $\chi_{\rm p} = 0.09^{+0.14}_{-0.07}$ for GW200105 and $\chi_{\rm p} = 0.21^{+0.30}_{-0.17}$ for GW200115. To assess the significance of a measurement of precession, we

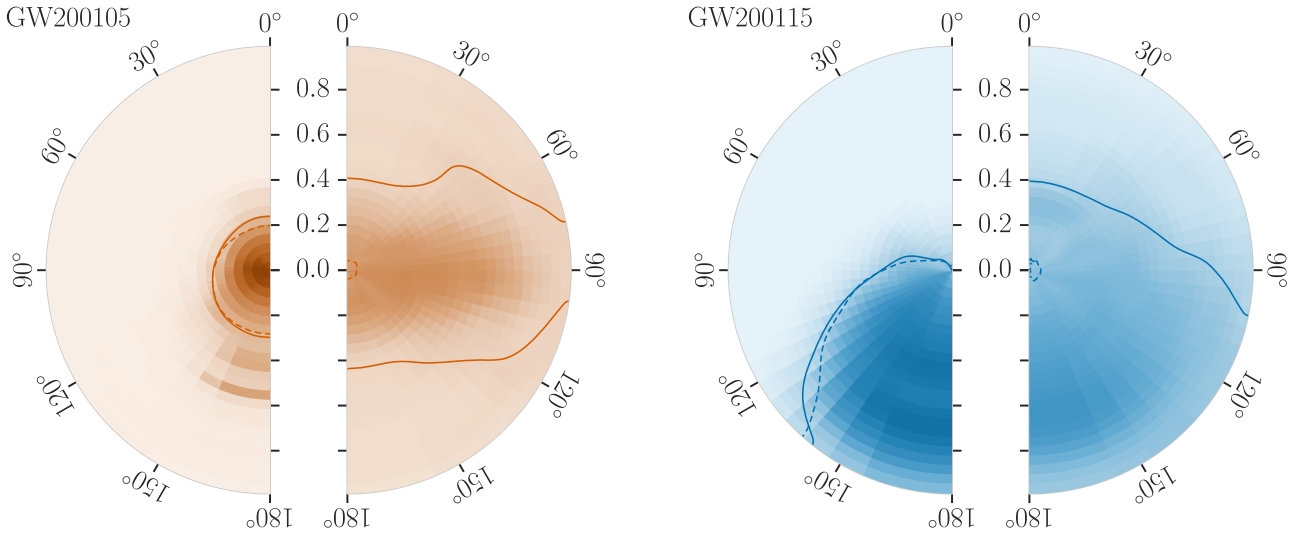

Figure 6. Two-dimensional posterior probability for the spin-tilt angle and spin magnitude for the primary objects (left hemispheres) and secondary objects (right hemispheres) for both events. Spin-tilt angles of 0° (180°) correspond to spins aligned (antialigned) with the orbital angular momentum. The color indicates the posterior probability per pixel of the high-spin prior analysis. For comparison with the low-spin analysis, the solid (dashed) lines indicate the 90% credible regions of the high-spin (low-spin) prior analyses. The tiles are constructed linearly in spin magnitude and cosine of the tilt angles such that each tile contains an identical prior probability. The probabilities are marginalized over the azimuthal angles.

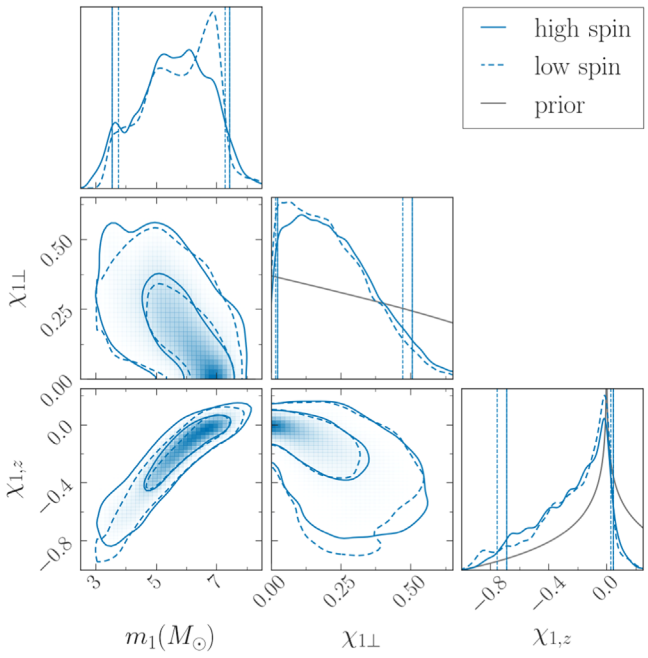

Figure 7. Properties of the primary component of GW200115. The corner plot shows the one-dimensional (diagonal) and two-dimensional (off-diagonal) marginal posterior distributions for the primary's mass and perpendicular and parallel spin components. The shading indicates the posterior probability of the high-spin prior analysis. The solid (dashed) lines indicate the 50% and 90% credible regions of the high-spin (low-spin) prior analyses. The vertical lines indicate the 90% credible intervals for the analyses with high-spin (solid lines) and low-spin (dashed lines) prior.

compute a Bayes factor between a precessing and nonprecessing signal model and the precession S/N ρ_p (Fairhurst et al. 2020a, 2020b). For GW200105, we find a log Bayes factor in favor of spin precession of $\log_{10}\mathcal{B} = -0.24$ and precession S/N $\rho_p = 0.74^{+1.35}_{-0.61}$. For GW200115, $\log_{10}\mathcal{B} = -0.12$ and $\rho_p = 0.97^{+1.57}_{-0.79}$. For both events and diagnostics, this indicates inconclusive evidence of precession. This result is expected given the S/Ns and inferred inclination angles of the binaries (Vitale et al. 2014; Green et al. 2020; Pratten et al. 2020c).

Low values of the primary mass of GW200115 ($m_1 \lesssim 5\,M_\odot$) are strongly correlated with negative values of the primary parallel spin component $\chi_{1,z}$, as shown in Figure 7. The astrophysical implications of the mass and spin correlation are discussed in Section 6. Figure 7 also shows the in-plane spin component $\chi_\perp$, which is peaked about zero. The lack of conclusive evidence for spin precession in GW200115 is consistent with the measurement of $\chi_\perp$. Apparent differences between the probability density of the primary spin in Figure 6 and the posteriors of $\chi_{1\perp}$–$\chi_{1,z}$ in Figure 7 arise from different choices in visualizing the spin orientation posteriors.

4.4. Remnant Properties

Under the hypothesis of NSBH coalescence for the two events, estimates for the final mass and spin of the remnant BH can be made using the models of Zappa et al. (2019). We use samples obtained by combining those from Phenom NSBH and EOB NSBH. For GW200105, the remnant mass and spin are $M_f = 10.4^{+2.7}_{-2.0}$ and $\chi_f = 0.43^{+0.04}_{-0.03}$, while for GW200115, $M_f = 7.8^{+1.4}_{-1.6}$ and $\chi_f = 0.38^{+0.04}_{-0.02}$. We do not investigate any postmerger GW signals. The S/Ns of GW200105 and GW200115 are around a factor of 3 less than that of GW170817, for which there was no evidence of GWs after the merger (Abbott et al. 2017b). In the absence of tidal disruption, the postmerger signals of GW200105 and GW200115 would likely resemble a BH ringdown (Foucart et al. 2013). The GW signal associated with such ringdowns would appear well outside of LIGO's and Virgo's sensitive bandwidth given the remnant masses and spins of the systems (Sarin & Lasky 2021).

4.5. Tests of General Relativity and Higher-order GW Multipole Moments

Results from parameterized tests of general relativity (GR; Blanchet & Sathyaprakash 1995; Yunes & Pretorius 2009; Mishra et al. 2010; Li et al. 2012a, 2012b; Agathos et al. 2014;

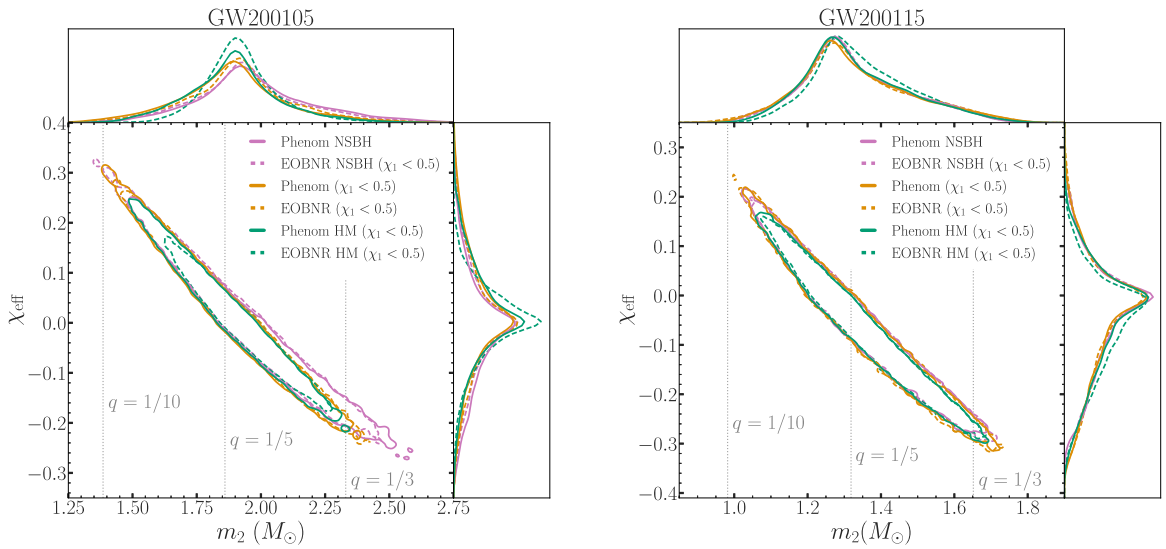

Figure 8. Comparison of two-dimensional m_2–$\chi_{\rm eff}$ posteriors for the two events reported here, using various NSBH and BBH signal models. The vertical dashed lines indicate several mass-ratio references mapped to m_2 for the median estimate of the chirp masses of GW200105 and GW200115.

Meidam et al. 2018; Abbott et al. 2019a) show that GW200105 and GW200115 have too low an S/N to allow for tighter constraints than those already presented in Abbott et al. (2021c). Within their measurement uncertainties, our results do not show statistically significant evidence for deviations from the prediction of GR.

To quantify the evidence for higher-order GW multipole moments, we calculate the orthogonal optimal S/N, $\rho^{\perp}_{lm}$, for the subdominant multipole moments (Abbott et al. 2020c, 2020d; Mills & Fairhurst 2021). We find $(\ell,\ |m|) = (3,\ 3)$ to be the loudest subdominant multipole moment, as expected for binaries with asymmetric masses. Using the Phenom HM waveform model, we infer $\rho^{\perp}_{33} = 1.70^{+0.92}_{-1.09}$ $(1.70^{+0.94}_{-1.11})$ for GW200105 and $\rho^{\perp}_{33} = 0.91^{+0.93}_{-0.66}$ $(0.86^{+0.90}_{-0.65})$ for GW200115 with the low (high) spin prior. In Gaussian noise, the median of $\rho^{\perp}_{33}$ is approximately χ-distributed with two degrees of freedom, and values greater than 2.1 indicate significant higher-order multipole content. The measured $\rho^{\perp}_{33}$ is therefore consistent with Gaussian noise, as expected for the majority of NSBHs at these S/Ns, except for those viewed close to edge-on.

4.6. Waveform Systematics

Our primary results are obtained using precessing BBH models with higher-order multipole moments, Phenom PHM and EOBNR PHM. We now justify this choice by investigating potential systematic uncertainties due to our waveform choice.

First, we investigate the agreement between independent waveform models that incorporate identical physics. Figure 8 shows the two-dimensional m_2–$\chi_{\rm eff}$ posteriors for both events obtained using a variety of NSBH and aligned-spin BBH models. Because some NSBH models only cover $\chi_1 < 0.5$, we restrict the prior range of all models to $\chi_1 < 0.5$ for consistency.

The main panels of Figure 8 are dominated by a correlation of the effective inspiral spin parameter $\chi_{\rm eff}$ with the secondary mass m_2 (Cutler & Flanagan 1994; Ng et al. 2018a). Both NSBH models (Phenom NSBH and EOBNR NSBH) give consistent results with each other, as do both BBH models (Phenom and EOBNR), both with and without higher-order multipole moments, with the most notable difference being that EOBNR HM yields tighter posteriors than Phenom HM. This demonstrates that waveform models including the same physics give comparable results, but more studies are warranted to improve the understanding of the BBH waveform models in the NSBH region of parameter space. While not shown in Figure 8, we also find good agreement between the primary precessing BBH waveform models; see Section 4.

Second, comparing the NSBH models with the BBH models without higher-order multipole moments (Phenom and EOBNR), the NSBH models recover similar posterior contours in the m_2–$\chi_{\rm eff}$ plane. This is expected given the asymmetric mass ratio and low S/N of these NSBH observations; see, e.g., Huang et al. (2021) for a demonstration that higher S/Ns would be needed to see notable systematic effects. We observe differences at the extreme ends of the m_2–$\chi_{\rm eff}$ contours (i.e., at the smallest and largest values of m_2). The construction of the NSBH waveform models used here did not rely on numerical relativity results at mass ratios $q \lesssim 1/8$, nor did they include simulations with $\chi_{1z} < 0$ or NS masses $m_2 > 1.4\ M_\odot$ (Matas et al. 2020; Thompson et al. 2020). Therefore, some differences should be expected, especially for large m_2 in GW200105. Furthermore, for GW200105, the tails of the m_2–$\chi_{\rm eff}$ distribution for Phenom NSBH and EOB NSBH at high m_2 are also impacted by the inability of the data to constrain the tidal deformability. Hence, the posterior samples include combinations of high m_2 with large Λ_2, despite such combinations being unphysical. This effect is not apparent for GW200115 because of its smaller secondary mass. The isolated islands of probability in the extreme tails of the distributions are due to sampling noise.

Last, when adding the extra physical content of higher-order multipole moments in BBH models (through Phenom HM and EOBNR HM), the extreme ends of the m_2–$\chi_{\rm eff}$ contours are excluded, while the bulk of the distributions are consistent with the posteriors obtained with the NSBH models. In summary, these comparisons indicate that (i) waveform models including the same physics give comparable results; (ii) going from NSBH models to comparable BBH models changes the results only marginally, i.e., any effects of tides are small; and (iii) inclusion of higher-order multipole moments changes the posterior contours more substantially than inclusion of tides.

Table 3
Probability that the Secondary Mass Is below the Maximum NS Mass $M_{\rm max}$ for Each Event, Given Different Spin Assumptions and Different Choices for the Maximum NS Mass

Spin Prior	Choice of $M_{\rm max}$	$p(m_2 < M_{\rm max})$	
		GW200105	GW200115
$\lvert\chi_2\rvert < 0.05$	$M_{\rm max,TOV}$	96%	98%
$\lvert\chi_2\rvert < 0.99$	$M_{\rm max}(\chi_2)$	94%	95%
$\lvert\chi_2\rvert < 0.99$	$M_{\rm max,GNS}$	93%	96%

Note. The values shown use a flat prior in m_2; alternative, astrophysically motivated mass priors can cause the estimates to vary by up to 11% across our chosen models.

We conclude that the inclusion of precession and higher-order multipole moments afforded by the BBH waveform models is more important than the impact of tides in the NSBH models.

5. Nature of the Secondary Components

In this section, we describe the investigations to establish the nature of the secondary objects. In Section 5.1, we look for imprints of tidal deformations of the secondaries and conclude that the masses, spins, distances, and S/Ns of the detections make definitive identifications of NSs unlikely in both GW and EM measurements. However, in Section 5.2, we show that the posterior distributions of the secondary masses agree with those of known NSs.

5.1. Tidal Deformability and Tidal Disruption

The tidal deformability of NSs is imprinted in the GW signal and investigated using the parameter estimation techniques of Section 4. In contrast, BHs have zero tidal deformability (Binnington & Poisson 2009; Damour & Nagar 2009; Chia 2020; Charalambous et al. 2021; Le Tiec & Casals 2021). We infer the tidal deformability Λ_2 of the NSs in GW200105 and GW200115 using the NSBH waveform models that include tides. We find that the tidal deformabilities are uninformative relative to a uniform prior in $\Lambda_2 \in [0, 5000]$. This measurement cannot establish the presence of NSs, which is expected given the mass ratios and S/N of the detections (Foucart et al. 2013; Kumar et al. 2017; Fasano et al. 2020; Huang et al. 2020).

Toward the end of the inspiral, the BH may tidally disrupt the NS and form an accretion disk (Pannarale 2013; Foucart et al. 2018). This is hypothesized to drive a relativistic jet (Pannarale et al. 2011; Paschalidis et al. 2015). Given the mass ratios for both events and the aligned spins $\chi_{1,z}$ of their primaries (near zero for GW200105, probably negative for GW200115), we do not expect tidal disruption to occur, which would require more equal masses or more positive $\chi_{1,z}$ (Rantsiou et al. 2008; Shibata & Taniguchi 2008; Etienne et al. 2009; Foucart et al. 2011, 2018; Kyutoku et al. 2011; Pannarale 2013).

To quantitatively confirm this expectation, we use the spectral representation of equations of state from Abbott et al. (2018a), which uses an SLY low-density crust model (Douchin & Haensel 2001) and parameterizes the adiabatic index into a polynomial in the logarithm of the pressure (Lindblom 2010; Lindblom & Indik 2012, 2014). Following Stachie et al. (2021), we marginalize the parameter estimation samples from the NSBH analyses over these equations of state. For a fixed equation of state, we compute the maximum Tolman–Oppenheimer–Volkov (TOV) mass, allowing us to infer the nature (NS or BH) of the lighter binary compact object, as well as its radius R_2, compactness $C_2 = Gm_2/(R_2c^2)$, and baryon mass. Based on these, we define a total ejecta mass $m_{\rm ej}$ (Fernández et al. 2019) as the sum of dynamical ejecta (Krüger & Foucart 2020) and 15% of the mass of disk winds (Foucart et al. 2018). For both events, we find that $m_{\rm ej} < 10^{-6}\,M_\odot$ for 99% of the samples.

The absence of ejecta is compatible with the lack of observed EM counterparts. However, given the large distances of the mergers ($\simeq$300 Mpc) and the large uncertainties of their sky localization, EM emission would have been difficult to detect and associate with these GW events.

Estimating the impact of nonlinear p–g tidal coupling (Abbott et al. 2019b), we find that it would produce a relative frequency-domain phase shift for GW200105 (GW200115) of approximately 134 (38) times smaller than the equivalent phase shift for GW170817. This strongly reduced effect is caused by the larger chirp masses, more asymmetric mass ratios, and the presence of only a single NS. Since p–g effects were not detected for GW170817 (Abbott et al. 2019b), they will be unobservable within the new NSBH systems.

5.2. Consistency of Component Masses with the NS Maximum Mass

Even without definite identification of matter signatures in the signals, we can compare the observed m_2 for GW200105 and GW200115 with the maximum NS mass, $M_{\rm max}$. The existence of massive pulsars (Antoniadis et al. 2013; Cromartie et al. 2019; Fonseca et al. 2021) places a lower bound of $M_{\rm max} \gtrsim 2\,M_\odot$ on the maximum NS mass. Studies of GW170817's remnant typically suggest that the maximum mass of a nonrotating NS—the TOV mass—is $M_{\rm max,TOV} \lesssim 2.3\,M_\odot$ (e.g., Shibata et al. 2019; Abbott et al. 2020b; Nathanail et al. 2021). However, rapid rotation could support a larger $M_{\rm max}$. Given the considerable uncertainty in $M_{\rm max}$, we examine three different scenarios. Following Essick & Landry (2020), we compute for each scenario the probability $p(m_2 < M_{\rm max})$ that the secondary mass is below the maximum NS mass by marginalizing over the uncertainty in $M_{\rm max}$ and the uncertainty of our m_2 measurement.

Supposing that the secondaries are slowly spinning, we consider in the first row of Table 3 an estimate of $M_{\rm max,TOV}$ from a nonparametric astrophysical inference of the equation of state (Landry et al. 2020), which predicts $M_{\rm max,TOV} = 2.22^{+0.30}_{-0.20}\,M_\odot$ and is shown in Figure 4. We then relax the low-spin assumption, estimating in the second row the maximum rotationally supported mass $M_{\rm max}(\chi_2)$ and the breakup spin $\chi_{\rm max}$ with the universal relations from Breu & Rezzolla (2016). In this scenario, we require $m_2 \leqslant M_{\rm max}(\chi_2)$ and $\chi_2 \leqslant \chi_{\rm max}$ for consistency with an NS. Finally, in the third row, we consider a parametric fit to the entire distribution of observed Galactic NSs, including rapidly rotating pulsars (Farr & Chatziioannou 2020), which predicts $M_{\rm max,GNS} = 2.25^{+0.71}_{-0.31}\,M_\odot$ and is shown in Figure 4. This scenario accounts for the possibility that the maximum mass in the NS population is limited by the astrophysical processes that form compact binaries. Assuming low spin (first row), we find probabilities of 96% and 98% that the secondaries in GW200105 and GW200115, respectively, are consistent with an NS assuming a uniform prior in m_2. The

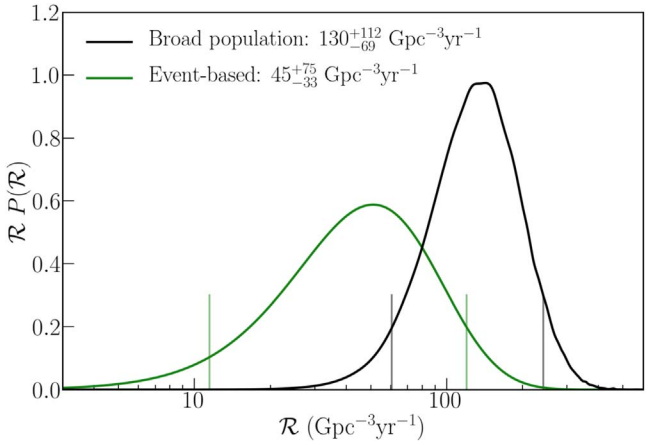

Figure 9. Inferred probability densities for the NSBH merger rate. Green line: rate assuming one count each from a GW200105- and GW200115-like NSBH population. Black line: rate for a broad NSBH population with a low threshold that accounts for marginal triggers. The short vertical lines indicate the 90% credible intervals.

possibility of large secondary spin reduces these probabilities by up to 3% (second and third rows).

So far, this analysis has assumed priors that are uniform in component masses. However, there is considerable uncertainty in the astrophysical mass priors of such systems, and different prior assumptions can affect the component mass posteriors for detections with moderate S/N. To illustrate the impact of population assumptions, we consider three alternative priors: one based on Salpeter mass distributions, $p(m) \sim m^{-2.3}$ (Salpeter 1955), independently for each component; one based on an extrapolation of the BBH mass model BROKEN POWER LAW from Abbott et al. (2021d) down to $0.5\,M_\odot$ for both components; and another based on a similar extrapolation of the POWER LAW + PEAK BBH mass model from the same study. We marginalize over the uncertainties in the latter two models, which are fit to the BBH population from Abbott et al. (2021b), including the outlier event GW190814 with a secondary component mass below $3\,M_\odot$ (Abbott et al. 2020c).

These different mass priors change the numbers in Table 3 by at most 11%, with the smallest values for GW200105 and GW200115 being 89% and 87%, respectively. The decrease is due to the three priors assigning more probability density to equal-mass systems, thus favoring larger m_2. Thus, the secondaries of both systems are consistent with NSs based on our assumptions about the equation of state and mass distribution.

However, consistency with the maximum NS mass does not exclude the possibility that the secondaries could be BHs or exotic compact objects, if such objects also exist within the NS mass range. For instance, models of primordial BHs predict a peak in the primordial BH mass function at $\sim 1\,M_\odot$ (Carr et al. 2021). These models also predict that primordial BHs may form coalescing binaries at mass ratios comparable to those reported here.

6. Astrophysical Implications

The first confident observations of NSBH binaries enable us to study this novel type of astrophysical system in entirely new ways. We pursue three different avenues in this section. First, we infer the merger rate of NSBH binaries in the local universe. We then place the inferred source properties and merger rate in the context of models of NSBH formation channels and previous EM and GW observations of BHs and NSs. Finally, we investigate to what extent the events reported here can serve to measure the Hubble constant and whether lensing of GWs may have played a role in the observations.

6.1. Merger Rate Density

We infer the NSBH merger rate density with our observations using two different approaches.

In the first approach, we consider only GW200105 and GW200115. Following the method of Kim et al. (2003) as previously used in, e.g., Abbott et al. (2016d, 2020c), we calculate an event-based merger rate assuming one Poisson-distributed count each from GW200105- and GW200115-like populations. We semianalytically calculate the search sensitivities across O1, O2, and the first 9 months of O3 to NSBH populations corresponding to the mass and spin posteriors for the two events. We then calibrate these sensitivities to the results of GSTLAL (Cannon et al. 2012; Privitera et al. 2014; Messick et al. 2017; Sachdev et al. 2019; Hanna et al. 2020) using a broad NSBH-like population and an FAR threshold of $1/(2.8\,\mathrm{yr})$. This FAR threshold is chosen to include only GW200105 and GW200115 while excluding low-significance triggers like GW190426_152155, though a more conservative threshold of $1/(100\,\mathrm{yr})$, as used in, e.g., Abbott et al. (2016d, 2020c), changes the estimated sensitivities by less than 15%. Applying the Poisson Jeffreys prior proportional to $\mathcal{R}_i^{-1/2}$, we find $\mathcal{R}_{200105} = 16^{+38}_{-14}\,\mathrm{Gpc}^{-3}\,\mathrm{yr}^{-1}$ and $\mathcal{R}_{200115} = 36^{+82}_{-30}\mathrm{Gpc}^{-3}\,\mathrm{yr}^{-1}$. The PYCBC detection of GW200115, using the same method but with an independent set of injections for calibration (Tiwari 2018), yields a consistent $\mathcal{R}_{200115} = 40^{+92}_{-34}$ $\mathrm{Gpc}^{-3}\,\mathrm{yr}^{-1}$. Combining the likelihoods over $\mathcal{R}_{200105}$ and $\mathcal{R}_{200115}$ according to Kim et al. (2003) and applying the Jeffreys prior to the total rate, we find the total event-based NSBH merger rate density $\mathcal{R}_{\mathrm{NSBH}} = 45^{+75}_{-33}$ $\mathrm{Gpc}^{-3}\,\mathrm{yr}^{-1}$, plotted in green in Figure 9.

The second approach to calculating a merger rate takes into account not only GW200105 and GW200115 but also less significant search triggers with masses consistent with the typical range associated with NSBH binaries. Specifically, we consider triggers across O1, O2, and the first 9 months of O3 with associated component masses $m_1 \in [2.5,\ 40]\ M_\odot$ and $m_2 \in [1,\ 3]\,M_\odot$, i.e., broader ranges than the component mass posteriors for GW200105 and GW200115 obtained in Section 4. The cutoff of $m_2 \leqslant 3\ M_\odot$ is chosen as a robust upper limit on the maximum NS mass (Rhoades & Ruffini 1974; Kalogera & Baym 1996). The population is defined to be uniformly distributed in comoving volume, uniform in log component masses in the given ranges, with aligned spins with spin magnitudes distributed uniformly in [0, 0.95]. We use as input GSTLAL search triggers above an S/N threshold such that the number of noise triggers exceeds the number of astrophysical signals by a factor of $\sim$100. Following Farr et al. (2015) and Kapadia et al. (2020), we find the resulting joint likelihood on Poisson parameters for signals of each astrophysical category (Λ_{BNS}, Λ_{NSBH}, Λ_{BBH}) and for terrestrial noise triggers $\Lambda_{\mathrm{background}}$. Here the BBH and BNS categories are defined to include triggers where both component masses fall within 5–100 or 1–2.5 $M_\odot$, respectively. We apply the Jeffreys prior and recover a merger rate density $\mathcal{R}_{\mathrm{NSBH}} = \Lambda_{\mathrm{NSBH}}/\langle VT\rangle_{\mathrm{NSBH}}$, where $\langle VT\rangle_{\mathrm{NSBH}}$ is the population-averaged sensitive time–volume estimated using the GSTLAL pipeline and the NSBH population defined above.

This yields an estimated NSBH merger rate density of $\mathcal{R}_{\rm NSBH} = 130^{+112}_{-69}\,{\rm Gpc^{-3}\,yr^{-1}}$, the black line in Figure 9.

While this rate is higher than our event-based rate, it considers a wider population that includes additional triggers; for example, the component masses of GW190814 (although the nature of its secondary is uncertain) fall within this population. The calculation is also based on the component mass values of GSTLAL search triggers, adjusted with an analytical model (Fong 2018) of the response of the template bank to signals with a given distribution of true masses. This procedure is expected to be less precise than Bayesian parameter estimation, which is impractical for the large numbers of triggers involved.

The merger rate density measured here is consistent with the upper bound of $610\,{\rm Gpc^{-3}\,yr^{-1}}$ derived from the absence of NSBH detections in O1 and O2 (Abbott et al. 2019c). Revised merger rate estimates for all CBC sources will be provided in a future analysis of the full O3 data set.

6.2. System Origins

To understand the origin of GW200105 and GW200115, we compare their observed masses and spins with theoretical predictions. Population synthesis studies modeling the various formation channels of merging compact object binaries distinguish between NSs and BHs with a simple mass cut, typically between 2 and 3 $M_\odot$. This is consistent with the secondary masses of both events being classified as NSs, so for the purposes of discussing formation channels for these events and predicted rates, we will discuss GW200105 and GW200115 in the context of them being NSBHs.

6.2.1. Formation Channels

Formation channels for NSBHs can be broadly categorized as either isolated binary evolution or one of several dynamical formation channels (e.g., globular clusters or nuclear star clusters). Since isolated binaries form in young star clusters and can be influenced by dynamical interactions before the cluster dissolves and the binary effectively becomes isolated, rates from young star clusters naturally encompass rates from isolated binaries. Predicted rates of NSBH mergers in the local universe vary by orders of magnitude across the various formation channels.

Models of the canonical isolated binary evolution channel—in which stellar progenitors evolve together, shedding orbital angular momentum through phases of stable and/or unstable mass transfer prior to compact object formation—predict NSBH merger rate densities around $0.1\text{–}800\,{\rm Gpc^{-3}\,yr^{-1}}$ (Belczynski et al. 2002; Sipior & Sigurdsson 2002; Belczynski et al. 2006, 2016; Dominik et al. 2015; Eldridge et al. 2017; Kruckow et al. 2018; Mapelli & Giacobbo 2018; Neijssel et al. 2019; Drozda et al. 2020; Zevin et al. 2020; Broekgaarden et al. 2021). The high uncertainty is driven by the lack of observed NSBHs and the wide range of model assumptions. Merger rates are sensitive to the treatment of common envelopes, which may be a necessary evolutionary phase for producing compact binaries in tight orbits capable of merging in a Hubble time (Ivanova et al. 2013). They are also sensitive to prescriptions for supernova kick magnitudes. While moderate kicks can produce eccentric orbits that merge on short timescales, high supernova kicks may disrupt the progenitor binaries and suppress the merger rate (Belczynski et al. 2002; Giacobbo & Mapelli 2020; Tang et al. 2020).

Models of star formation in the dynamical environments of young star clusters predict NSBH merger rate densities of $0.1\text{–}100\,{\rm Gpc^{-3}\,yr^{-1}}$ (Fragione & Banerjee 2020; Hoang et al. 2020; Rastello et al. 2020; Santoliquido et al. 2020). In this scenario, most systems that form merging NSBHs ($\sim$80%) are ejected without undergoing dynamical exchanges, proceeding to merge in the field.

Models of dynamical formation channels in denser environments typically predict much lower merger rates. For instance, in globular clusters and nuclear star clusters, BHs segregate and dominate the core, where the bulk of dynamical interactions occur (Portegies Zwart & McMillan 2000; Morscher et al. 2015), so that encounters between NSs and BHs are relatively rare, with NSBH merger rate densities on the order of 10^{-2} $\rm Gpc^{-3}\,yr^{-1}$ (Clausen et al. 2013; Arca Sedda 2020; Ye et al. 2020). In disks of active galactic nuclei, the presence of gas could possibly increase the NSBH merger rate density up to $300\ {\rm Gpc^{-3}\ yr^{-1}}$ (McKernan et al. 2020).

NSBHs may also merge via hierarchical triple interactions, where inner NSBH binaries are driven to high eccentricity by massive tertiary companions and merge on rapid timescales (Antonini et al. 2017; Silsbee & Tremaine 2017). However, the predicted merger rates are negligible unless supernova kicks are assumed to be zero (Fragione & Loeb 2019).

It is likely that a combination of the above channels contribute to the astrophysical NSBH merger rate. However, the isolated binary evolution, young star cluster, and active galactic nuclei channels are capable of individually accounting for the NSBH merger rate estimated here.

6.2.2. Masses

While there are no observed NSBHs in the Milky Way, we can place the component masses of GW200105 and GW200115 in the context of the observed population of BH and NS masses, as well as the predicted populations of NSBHs. Observations suggest that the mass distribution of the Galactic population of NSs peaks around $1.33\,M_\odot$, with a secondary peak around $1.9\,M_\odot$ (Antoniadis et al. 2016; Alsing et al. 2018). The secondary mass observed in GW200115 and marginal event GW190426_152155 are consistent with the population peaking at $1.33\,M_\odot$, while the secondary observed in GW200105 ($\simeq 1.9\,M_\odot$) and the primary component from BNS merger GW190425 ($m_1 = $ 1.60–1.87 $M_\odot$; Abbott et al. 2020b) are consistent with the high-mass population. However, a rigorous association of the events with different components of the NS population would require a thorough population analysis. Radio observations of BNS systems do not find such massive NSs, leading to speculation as to the origin of GW190425 (Romero-Shaw et al. 2020a; Safarzadeh et al. 2020; Galaudage et al. 2021; Mandel et al. 2021). Stellar metallicities in the Milky Way are not representative of all populations of GW sources (O'Shaughnessy et al. 2008, 2010; Belczynski et al. 2010; Eldridge et al. 2017; Neijssel et al. 2019).

The BH masses observed in GW200105 and GW200115 ($8.9^{+1.2}_{-1.5}$ and $5.7^{+1.8}_{-2.1}\,M_\odot$, respectively) are in line with predictions from population synthesis models for NSBH mergers from isolated binary evolution and young star clusters. In NSBHs, current binary evolution models do not predict BH masses above $\simeq 10\ M_\odot$ (Eldridge et al. 2017; Kruckow et al.

2018; Mapelli & Giacobbo 2018; Broekgaarden et al. 2021), while Population III NSBHs (Kinugawa et al. 2017) and dynamical interactions in low-metallicity young star clusters allow for higher BH masses (Ziosi et al. 2014; Rastello et al. 2020).

Electromagnetic observations of X-ray binaries have not uncovered BHs between 3 and 5 $M_\odot$, leading to speculation about a mass gap (Özel et al. 2010; Farr et al. 2011; Kreidberg et al. 2012; Miller & Miller 2014). Analysis of GWTC-2 has also found evidence for a gap or dip in the BH mass spectrum between $\sim$2.6 and $4\,M_\odot$ (Fishbach et al. 2020). For GW200115, we find nonnegligible support for the primary lying in this mass gap, with $p(3\,M_\odot < m_1 < 5\,M_\odot) = 30\%$ (27%) under the high-spin (low-spin) priors. This low-mass region is correlated with negative values of the parallel component of the primary spin; see Section 6.2.3 below.

In summary, the masses inferred for GW200105 and GW200115 are consistent with expectations for NSBHs; their primary masses are in agreement with predictions for BH masses in population synthesis models of the dominant formation scenarios. Meanwhile, their secondary masses are compatible with the observed population of Galactic NSs, as well as the masses inferred from GW observations of BNS mergers.

6.2.3. Spins

Spin information encoded in GWs from binaries is a probe of their evolutionary history (Farr et al. 2017, 2018; Stevenson et al. 2017; Talbot & Thrane 2017; Vitale et al. 2017c; Wysocki et al. 2019). The BHs in binaries are expected to exhibit a range of spin magnitudes and orientations, depending on how they formed (Mandel & O'Shaughnessy 2010; Rodriguez et al. 2016; Liu & Lai 2017, 2018; Antonini et al. 2018; Kruckow et al. 2018; Bavera et al. 2020; Chattopadhyay et al. 2020; Kalogera 2000). The highest dimensionless NS spin implied by pulsar-timing observations of binaries that merge within a Hubble time is $\sim$0.04 (Stovall et al. 2018; Zhu et al. 2018).

While the secondary spins of both events reported here are poorly constrained due to the unequal masses, the primary spins of GW200105 and GW200115 can be placed in the context of predictions for BH spins from models of stellar and dynamical evolution and EM observations of NSBH progenitors. As can be seen in Figures 6 and 7, the primary spins of GW200105 and GW200115 are consistent with zero ($0.08^{+0.22}_{-0.08}$ and $0.33^{+0.48}_{-0.29}$, respectively), but moderate values of spin are not ruled out. The primary in GW200115 may even have relatively high spin, with a 90% upper limit of 0.72. Several studies of the observed population of high-mass X-ray binaries (Liu et al. 2008; Gou et al. 2009, 2014; Zhao et al. 2021) find that the BHs have large spins (Valsecchi et al. 2010; Wong et al. 2012; Qin et al. 2019; Zhao et al. 2021). Given the short lifetime of the secondary, mass transfer is argued to be insufficient to generate BHs with such high spins, implying that the BHs were born with high spins. Belczynski et al. (2011) found that one such high-mass X-ray binary, Cygnus X-1, is expected to form an NSBH with a BH that carries near-maximal spin, although it would not merge within a Hubble time. However, following revised estimates of the component masses of Cygnus X-1 (Miller-Jones et al. 2021), Neijssel et al. (2021) found that it will most likely form a BBH. Meanwhile, analyses of GWTC-1 and GWTC-2 have found evidence for BH spin (Abbott et al. 2016f, 2021d; Vitale et al. 2017a; Chatziioannou et al. 2019; Kimball et al. 2020), though they do not determine whether those BHs may have been formed with that spin. Altogether, these EM and GW observations of compact binaries and their progenitors suggest a range of BH natal spins in NSBH binaries.

Along with their magnitudes, the alignments of component spins with the overall binary orbital angular momentum are of astrophysical interest. In particular, we find evidence that the primary BH spin in GW200115 is negatively aligned with respect to the orbital angular momentum axis, with $p(\chi_{1,z} < 0) = 88\%$ (87%) under the high-spin (low-spin) prior and the more negative values of $\chi_{1,z}$ correlated with smaller m_1. This negative alignment is consistent with dynamical formation channels, which typically form binaries with random spin orientations (Rodriguez et al. 2016), but the predicted rates from these channels, discussed in Section 6.2, are small. Binaries born in isolation are expected to form with only small misalignments ($\lesssim 30^\circ$; Kalogera 2000), though they may become misaligned by supernova kicks at compact object formation (Rodriguez et al. 2016; Gerosa et al. 2018; Wysocki et al. 2018) and possibly during subsequent evolution via mass transfer (Stegmann & Antonini 2021). Meanwhile, NSBH progenitor binaries originating in young star clusters can be perturbed via close dynamical encounters before being ejected into the field. Therefore, a misaligned spin in the primary of GW200115 would not necessarily rule out any of the plausible NSBH formation channels.

6.3. Cosmology and Lensing

Gravitational wave sources are standard sirens, providing a direct measurement of their luminosity distance (Schutz 1986; Holz & Hughes 2005), and they can be used to measure the Hubble constant (Abbott et al. 2017c, 2021a; Fishbach et al. 2019). Due to the lack of a confirmed EM counterpart and large numbers of galaxies inside the localization volumes of each of the two events, we do not obtain any informative bounds on H_0 from these observations.

The detections of GW200105 and GW200115 are separated by only $\sim$10 days. One explanation for the small time delay could be that the two events are created by gravitational lensing by a galaxy (Haris et al. 2018). Gravitational lensing is unlikely even a priori (Smith et al. 2017; Ng et al. 2018b), and the nonoverlapping mass posteriors (Figure 4) further exclude it as a possible explanation (Haris et al. 2018). While GW200115 and GW190426_152155 exhibit agreement in their source mass posteriors, their sky localization areas do not overlap, and their detector-frame (redshifted) chirp masses show only marginal overlap (Abbott et al. 2021b), ruling out lensing as a possible explanation.

7. Conclusions

During its third observing run, the LIGO–Virgo GW detector network observed GW200105 and GW200115, two GW events consistent with NSBH coalescences. Event GW200105 is effectively a single-detector event observed in LIGO Livingston with an S/N of 13.9. It clearly stands apart from all recorded noise transients, but its statistical confidence is difficult to establish. Event GW200115 was observed in coincidence by the network with an S/N of 11.6 and FAR of $<1/(1\times10^5\,\mathrm{yr})$.

The source component masses of GW200105 and GW200115 make it likely that these events originated from NSBH coalescences. Their primary masses are found to be $m_1 = 8.9^{+1.2}_{-1.5}$ and $5.7^{+1.8}_{-2.1}\,M_\odot$, which are consistent with predictions of BH masses in population synthesis models for NSBHs. Their secondary masses, inferred to be $m_2 = 1.9^{+0.3}_{-0.2}$ and $1.5^{+0.7}_{-0.3}\,M_\odot$, respectively, are consistent with the observed NS mass distribution in the Milky Way, as well as population synthesis predictions for secondary masses in merging NSBHs.

We find no evidence of measurable tides or tidal disruption for either of the two signals, and no EM counterparts to either detection have been identified. As such, there is no direct evidence that the secondaries are NSs, and our observations are consistent with either event being a BBH merger. However, the absence of tidal measurements and EM counterparts is to be expected given the properties and distances of the two events. Moreover, the comparisons of the secondary masses to the maximum allowed NS mass yield a probability $p(m_2 \leqslant M_{\rm max})$ of 89%–96% and 87%–98% for the secondaries in GW200105 and GW200115, respectively, being compatible with NSs (see Section 5.2).

The effective inspiral spin parameter of GW200105 is strongly peaked around zero: $\chi_{\rm eff} = -0.01^{+0.11}_{-0.15}$. For the second event, GW200115, the effective inspiral spin parameter is inferred to be $\chi_{\rm eff} = -0.19^{+0.23}_{-0.35}$. For GW200115, the spin component parallel to the orbital angular momentum of the primary is $\chi_{1,z} = -0.19^{+0.24}_{-0.50}$, and we find support for negatively aligned primary spin ($\chi_{1,z} < 0$) at 88% probability. More negative values of $\chi_{1,z}$ in GW200115 are correlated with particularly small primary masses reaching into the lower mass gap. We find $p(3\,M_\odot < m_1 < 5\,M_\odot) = 30\%$ (27%) under the high-spin (low-spin) parameter estimation priors. We find no conclusive evidence for spin-induced orbital precession in either system.

We estimate the merger rate density of NSBH binaries with two approaches. Assuming that GW200105 and GW200115 are representative of the entire NSBH population, we find $\mathcal{R}_{\rm NSBH} = 45^{+75}_{-33}\ {\rm Gpc^{-3}\,yr^{-1}}$. Conversely, assuming a broader range of allowed primary and secondary masses, and considering all triggers in O3, we find $\mathcal{R}_{\rm NSBH} = 130^{+112}_{-69}\ {\rm Gpc^{-3}\,yr^{-1}}$. These are the first direct measurements of the NSBH merger rate. Both estimates are broadly consistent with the rate predicted from NSBH formation in isolated binaries or via young star clusters. Formation channels in dense star clusters (globular or nuclear) and triples predict lower rates than those inferred from the two events and are unlikely to be the dominant NSBH formation channels.

The observations of GW200105 and GW200115 are consistent with predictions for merging NSBHs and observations of BHs and NSs in the Milky Way. Given their significantly unequal component masses, future observations of NSBH systems will provide new opportunities to study matter under extreme conditions, including tidal disruption, and search for potential deviations from GR.

This material is based upon work supported by the NSF's LIGO Laboratory, which is a major facility fully funded by the National Science Foundation. The authors also gratefully acknowledge the support of the Science and Technology Facilities Council (STFC) of the United Kingdom, the Max Planck Society (MPS), and the State of Niedersachsen/Germany for support of the construction of Advanced LIGO and construction and operation of the GEO600 detector. Additional support for Advanced LIGO was provided by the Australian Research Council. The authors gratefully acknowledge the Italian Istituto Nazionale di Fisica Nucleare (INFN), the French Centre National de la Recherche Scientifique (CNRS), and the Netherlands Organization for Scientific Research for the construction and operation of the Virgo detector and the creation and support of the EGO consortium. The authors also gratefully acknowledge research support from these agencies, as well as the Council of Scientific and Industrial Research of India, the Department of Science and Technology, India, the Science & Engineering Research Board (SERB), India, the Ministry of Human Resource Development, India, the Spanish Agencia Estatal de Investigación, the Vicepresidència i Conselleria d'Innovació Recerca i Turisme and the Conselleria d'Educació i Universitat del Govern de les Illes Balears, the Conselleria d'Innovació Universitats, Ciència i Societat Digital de la Generalitat Valenciana and the CERCA Programme Generalitat de Catalunya, Spain, the National Science Centre of Poland and the Foundation for Polish Science (FNP), the Swiss National Science Foundation (SNSF), the Russian Foundation for Basic Research, the Russian Science Foundation, the European Commission, the European Regional Development Funds (ERDF), the Royal Society, the Scottish Funding Council, the Scottish Universities Physics Alliance, the Hungarian Scientific Research Fund (OTKA), the French Lyon Institute of Origins (LIO), the Belgian Fonds de la Recherche Scientifique (FRS-FNRS), Actions de Recherche Concertés (ARC) and Fonds Wetenschappelijk Onderzoek—Vlaanderen (FWO), Belgium, the Paris Île-de-France Region, the National Research, Development and Innovation Office Hungary (NKFIH), the National Research Foundation of Korea, the Natural Science and Engineering Research Council Canada, Canadian Foundation for Innovation (CFI), the Brazilian Ministry of Science, Technology, and Innovations, the International Center for Theoretical Physics South American Institute for Fundamental Research (ICTP-SAIFR), the Research Grants Council of Hong Kong, the National Natural Science Foundation of China (NSFC), the Leverhulme Trust, the Research Corporation, the Ministry of Science and Technology (MOST), Taiwan, the United States Department of Energy, and the Kavli Foundation. The authors gratefully acknowledge the support of the NSF, STFC, INFN, and CNRS for provision of computational resources.

This work was supported by MEXT, the JSPS Leading-edge Research Infrastructure Program, JSPS Grant-in-Aid for Specially Promoted Research 26000005, JSPS Grant-in-Aid for Scientific Research on Innovative Areas 2905: JP17H06358, JP17H06361, and JP17H06364, JSPS Core-to-Core Program A. Advanced Research Networks, JSPS Grant-in-Aid for Scientific Research (S) 17H06133, the joint research program of the Institute for Cosmic Ray Research, University of Tokyo, National Research Foundation (NRF) and Computing Infrastructure Project of KISTI-GSDC in Korea, Academia Sinica (AS), AS Grid Center (ASGC) and the Ministry of Science and Technology (MoST) in Taiwan under grants including AS-CDA-105-M06, Advanced Technology Center (ATC) of NAOJ, and Mechanical Engineering Center of KEK.

Some of the parameter estimation analyses presented in this paper were performed using supercomputer clusters at Swinburne University of Technology (OzSTAR and SSTAR), Cardiff University (ARCCA), the Max Planck Institute for

Gravitational Physics (Hypatia), and the Barcelona Supercomputing Center—Centro Nacional de Supercomputación.

We would like to thank all of the essential workers who put their health at risk during the COVID-19 pandemic, without whom we would not have been able to complete this work.

Software: The detection of the signal and subsequent significance evaluation were performed with the GSTLAL-based inspiral software pipeline (Cannon et al. 2012; Privitera et al. 2014; Messick et al. 2017; Sachdev et al. 2019; Hanna et al. 2020), built on the LALSUITE software library (LIGO Scientific Collaboration 2018), and with the PYCBC (Usman et al. 2016; Nitz et al. 2018, 2019a) and MBTA ONLINE (Adams et al. 2016) packages. Parameter estimation was performed with the LALINFERENCE (Veitch et al. 2015) and LALSIMULATION libraries within LALSUITE (LIGO Scientific Collaboration 2018), as well as the BILBY and PBILBY Libraries (Ashton et al. 2019; Smith et al. 2020) and the DYNESTY nested sampling package (Speagle 2020). Estimates of the noise spectra were obtained using BAYESWAVE (Cornish & Littenberg 2015; Littenberg & Cornish 2015). Parameter estimation results were visualized and shared with the PESUMMARY software library (Hoy & Raymond 2020). Plots were prepared with Matplotlib (Hunter 2007). Figure 1 was generated using GWpy (Macleod et al. 2020). The sky map plot also used Astropy (http://www.astropy.org), a community-developed core Python package for astronomy (Robitaille et al. 2013; Price-Whelan et al. 2018), and `ligo.skymap` (https://lscsoft.docs.ligo.org/ligo.skymap).

References

Abbott, B. P., Abbott, R., Abbott, T. D., et al. 2016a, PhRvX, 6, 041015
Abbott, B. P., Abbott, R., Abbott, T. D., et al. 2016b, PhRvD, 93, 122003
Abbott, B. P., Abbott, R., Abbott, T. D., et al. 2016c, PhRvL, 116, 241102
Abbott, B. P., Abbott, R., Abbott, T. D., et al. 2016d, ApJL, 833, L1
Abbott, B. P., Abbott, R., Abbott, T. D., et al. 2016e, CQGra, 33, 134001
Abbott, B. P., Abbott, R., Abbott, T. D., et al. 2016f, PhRvL, 116, 241103
Abbott, B. P., Abbott, R., Abbott, T. D., et al. 2017a, PhRvL, 119, 161101
Abbott, B. P., Abbott, R., Abbott, T. D., et al. 2017b, ApJL, 851, L16
Abbott, B. P., Abbott, R., Abbott, T. D., et al. 2017c, Natur, 551, 85
Abbott, B. P., Abbott, R., Abbott, T. D., et al. 2018a, PhRvL, 121, 161101
Abbott, B. P., Abbott, R., Abbott, T. D., et al. 2018b, CQGra, 35, 065010
Abbott, B. P., Abbott, R., Abbott, T. D., et al. 2019a, PhRvL, 123, 011102
Abbott, B. P., Abbott, R., Abbott, T. D., et al. 2019b, PhRvL, 122, 061104
Abbott, B. P., Abbott, R., Abbott, T. D., et al. 2019c, PhRvX, 9, 031040
Abbott, B. P., Abbott, R., Abbott, T. D., et al. 2020a, ApJL, 892, L3
Abbott, B. P., Abbott, R., Abbott, T. D., et al. 2020b, CQGra, 37, 045006
Abbott, B. P., Abbott, R., Abbott, T. D., et al. 2021a, ApJ, 909, 218
Abbott, R., Abbott, T. D., Abraham, S., et al. 2020c, ApJL, 896, L44
Abbott, R., Abbott, T. D., Abraham, S., et al. 2020d, PhRvD, 102, 043015
Abbott, R., Abbott, T. D., Abraham, S., et al. 2021b, PhRvX, 11, 021053
Abbott, R., Abbott, T. D., Abraham, S., et al. 2021c, PhRvD, 103, 122002
Abbott, R., Abbott, T. D., Abraham, S., et al. 2021d, ApJL, 913, L7
Acernese, F., Adams, T., Agatsuma, K., et al. 2018, CQGra, 35, 205004
Adams, T., Buskulic, D., Germain, V., et al. 2016, CQGra, 33, 175012
Ade, P. A. R., Aghanim, N., Arnaud, M., et al. 2016, A&A, 594, A13
Agathos, M., Del Pozzo, W., Li, T. G. F., et al. 2014, PhRvD, 89, 082001
Agazie, G., Mingyar, M., McLaughlin, M., et al. 2021, arXiv:2102.10214
Ajith, P., Fotopoulos, N., Privitera, S., Neunzert, A., & Weinstein, A. J. 2014, PhRvD, 89, 084041
Allen, B., Anderson, W. G., Brady, P. R., Brown, D. A., & Creighton, J. D. E. 2012, PhRvD, 85, 122006
Alsing, J., Silva, H. O., & Berti, E. 2018, MNRAS, 478, 1377
Antoniadis, J., Freire, P. C. C., Wex, N., et al. 2013, Sci, 340, 1233232
Antoniadis, J., Tauris, T. M., Ozel, F., et al. 2016, arXiv:1605.01665
Antonini, F., Rodriguez, C. L., Petrovich, C., & Fischer, C. L. 2018, MNRAS, 480, L58
Antonini, F., Toonen, S., & Hamers, A. S. 2017, ApJ, 841, 77
Apostolatos, T. A., Cutler, C., Sussman, G. J., & Thorne, K. S. 1994, PhRvD, 49, 6274
Arca Sedda, M. 2020, CmPhy, 3, 43
Ashton, G., Hübner, M., Lasky, P. D., et al. 2019, ApJS, 241, 27
Ashton, G., & Khan, S. 2020, PhRvD, 101, 064037
Aubin, F., Brighenti, F., Chierici, R., et al. 2021, CQGra, 38, 095004
Babak, S. 2008, CQGra, 25, 195011
Bailyn, C. D., Jain, R. K., Coppi, P., & Orosz, J. A. 1998, ApJ, 499, 367
Bavera, S. S., Fragos, T., Qin, Y., et al. 2020, A&A, 635, A97
Belczynski, K., Bulik, T., & Bailyn, C. 2011, ApJL, 742, L2
Belczynski, K., Bulik, T., Mandel, I., et al. 2013, ApJ, 764, 96
Belczynski, K., Dominik, M., Bulik, T., et al. 2010, ApJL, 715, L138
Belczynski, K., Kalogera, V., & Bulik, T. 2002, ApJ, 572, 407
Belczynski, K., Perna, R., Bulik, T., et al. 2006, ApJ, 648, 1110
Belczynski, K., Repetto, S., Holz, D. E., et al. 2016, ApJ, 819, 108
Binnington, T., & Poisson, E. 2009, PhRvD, 80, 084018
Blanchet, L., & Sathyaprakash, B. 1995, PhRvL, 74, 1067
Bohé, A., Shao, L., Taracchini, A., et al. 2017, PhRvD, 95, 044028
Breu, C., & Rezzolla, L. 2016, MNRAS, 459, 646
Broekgaarden, F. S., Berger, E., Neijssel, C. J., et al. 2021, arXiv:2103.02608
Burgay, M., D'Amico, N., Possenti, A., et al. 2003, Natur, 426, 531
Callister, T. A., Kanner, J. B., Massinger, T. J., Dhurandhar, S., & Weinstein, A. J. 2017, CQGra, 34, 155007
Cannon, K., Cariou, R., Chapman, A., et al. 2012, ApJ, 748, 136
Carr, B., Clesse, S., García-Bellido, J., & Kühnel, F. 2021, PDU, 31, 100755
Charalambous, P., Dubovsky, S., & Ivanov, M. M. 2021, JHEP, 2021, 38
Chatterjee, D., Ghosh, S., Brady, P. R., et al. 2020, ApJ, 896, 54
Chatterji, S., Blackburn, L., Martin, G., & Katsavounidis, E. 2004, CQGra, 21, S1809
Chattopadhyay, D., Stevenson, S., Hurley, J. R., Bailes, M., & Broekgaarden, F. 2020, arXiv:2011.13503
Chatziioannou, K., Cotesta, R., Ghonge, S., et al. 2019, PhRvD, 100, 104015
Chia, H. S. 2020, arXiv:2010.07300
Chu, Q., Kovalam, M., Wen, L., et al. 2020, arXiv:2011.06787
Clausen, D., Sigurdsson, S., & Chernoff, D. F. 2013, MNRAS, 428, 3618
Cornish, N. J., & Littenberg, T. B. 2015, CQGra, 32, 135012
Cornish, N. J., Littenberg, T. B., Bécsy, B., et al. 2021, PhRvD, 103, 044006
Cotesta, R., Buonanno, A., Bohé, A., et al. 2018, PhRvD, 98, 084028
Cotesta, R., Marsat, S., & Pürrer, M. 2020, PhRvD, 101, 124040
Cromartie, H. T., Fonseca, E., Ransom, S. M., et al. 2019, NatAs, 4, 72
Cutler, C., & Flanagan, E. E. 1994, PhRvD, 49, 2658
Dal Canton, T., Nitz, A. H., Gadre, B., et al. 2020, arXiv:2008.07494
Damour, T. 2001, PhRvD, 64, 124013
Damour, T., & Nagar, A. 2009, PhRvD, 80, 084035
Davis, D., Areeda, J. S., Berger, B. K., et al. 2021, CQGra, 38, 135014
Dexheimer, V., Gomes, R. O., Klähn, T., Han, S., & Salinas, M. 2021, PhRvC, 103, 025808
Dominik, M., Berti, E., O'Shaughnessy, R., et al. 2015, ApJ, 806, 263
Douchin, F., & Haensel, P. 2001, A&A, 380, 151
Drozda, P., Belczynski, K., O'Shaughnessy, R., Bulik, T., & Fryer, C. L. 2020, arXiv:2009.06655
Eldridge, J. J., Stanway, E. R., Xiao, L., et al. 2017, PASA, 34, e058
Essick, R., & Landry, P. 2020, ApJ, 904, 80
Etienne, Z. B., Liu, Y. T., Shapiro, S. L., & Baumgarte, T. W. 2009, PhRvD, 79, 044024
Fairhurst, S., Green, R., Hannam, M., & Hoy, C. 2020a, PhRvD, 102, 041302
Fairhurst, S., Green, R., Hoy, C., Hannam, M., & Muir, A. 2020b, PhRvD, 102, 024055
Farr, B., Holz, D. E., & Farr, W. M. 2018, ApJL, 854, L9
Farr, W. M., & Chatziioannou, K. 2020, RNAAS, 4, 65
Farr, W. M., Sravan, N., Cantrell, A., et al. 2011, ApJ, 741, 103
Farr, W. M., Stevenson, S., Miller, M. C., et al. 2017, Natur, 548, 426
Farr, W. M., Gair, J. R, Mandel, I., & Cutler, C. 2015, PhRvD, 91, 023005
Farrow, N., Zhu, X.-J., & Thrane, E. 2019, ApJ, 876, 18
Fasano, M., Wong, K. W., Maselli, A., et al. 2020, PhRvD, 102, 023025
Fattoyev, F. J., Horowitz, C. J., Piekarewicz, J., & Reed, B. 2020, PhRvC, 102, 065805
Fernández, R., Tchekhovskoy, A., Quataert, E., Foucart, F., & Kasen, D. 2019, MNRAS, 482, 3373
Fishbach, M., Essick, R., & Holz, D. E. 2020, ApJL, 899, L8
Fishbach, M., Gray, R., Magaña Hernandez, I., et al. 2019, ApJL, 871, L13
Fong, H. K. Y. 2018, PhD thesis, Toronto Univ.
Fonseca, E., Cromartie, H. T., Pennucci, T. T., et al. 2021, arXiv:2104.00880
Foucart, F., Buchman, L., Duez, M. D., et al. 2013, PhRvD, 88, 064017
Foucart, F., Duez, M. D., Kidder, L. E., & Teukolsky, S. A. 2011, PhRvD, 83, 024005

Foucart, F., Hinderer, T., & Nissanke, S. 2018, PhRvD, 98, 081501
Fragione, G., & Banerjee, S. 2020, ApJL, 901, L16
Fragione, G., & Loeb, A. 2019, MNRAS, 486, 4443
Galaudage, S., Adamcewicz, C., Zhu, X.-J., Stevenson, S., & Thrane, E. 2021, ApJL, 909, L19
García-Quirós, C., Colleoni, M., Husa, S., et al. 2020, PhRvD, 102, 064002
GCN archive for S200105ae 2020, GCN Archive for S200105ae, https://gcn.gsfc.nasa.gov/other/S200105ae.gcn3
GCN archive for S200115j 2020, GCN Archive for S200115j, https://gcn.gsfc.nasa.gov/other/S200115j.gcn3
Gerosa, D., Berti, E., O'Shaughnessy, R., et al. 2018, PhRvD, 98, 084036
Giacobbo, N., & Mapelli, M. 2020, ApJ, 891, 141
Godzieba, D. A., Radice, D., & Bernuzzi, S. 2021, ApJ, 908, 122
Gou, L., McClintock, J. E., Liu, J., et al. 2009, ApJ, 701, 1076
Gou, L., McClintock, J. E., Remillard, R. A., et al. 2014, ApJ, 790, 29
Green, R., Hoy, C., Fairhurst, S., et al. 2020, PhRvD, 12, 124023
Grudzinska, M., Belczynski, K., Casares, J., et al. 2015, MNRAS, 452, 2773
Guo, X., Chu, Q., Chung, S. K., et al. 2018, CoPhC, 231, 62
Hanna, C., Caudill, S., Messick, C., et al. 2020, PhRvD, 101, 022003
Haris, K., Mehta, A. K., Kumar, S., Venumadhav, T., & Ajith, P. 2018, arXiv:1807.07062
Harry, I. W., Allen, B., & Sathyaprakash, B. S. 2009, PhRvD, 80, 104014
Hoang, B.-M., Naoz, S., & Kremer, K. 2020, ApJ, 903, 8
Holz, D. E., & Hughes, S. A. 2005, ApJ, 629, 15
Hooper, S., Chung, S. K., Luan, J., et al. 2012, PhRvD, 86, 024012
Hoy, C., & Raymond, V. 2020, arXiv:2006.06639
Huang, Y., Haster, C.-J., Roulet, J., et al. 2020, PhRvD, 102, 103024
Huang, Y., Haster, C.-J., Vitale, S., et al. 2021, PhRvD, 103, 083001
Hunter, J. D. 2007, CSE, 9, 90
Ivanova, N., Justham, S., Chen, X., et al. 2013, A&ARv, 21, 59
Kalogera, V. 2000, ApJ, 541, 319
Kalogera, V., & Baym, G. 1996, ApJL, 470, L61
Kapadia, S. J., Caudill, S., Creighton, J. D. E., et al. 2020, CQGra, 37, 045007
Kim, C., Kalogera, V., & Lorimer, D. R. 2003, ApJ, 584, 985
Kimball, C., Talbot, C. L., Berry, C. P., et al. 2020, ApJ, 900, 177
Kinugawa, T., Nakamura, T., & Nakano, H. 2017, PTEP, 2017, 021E01
Kreidberg, L., Bailyn, C. D., Farr, W. M., & Kalogera, V. 2012, ApJ, 757, 36
Kruckow, M. U., Tauris, T. M., Langer, N., Kramer, M., & Izzard, R. G. 2018, MNRAS, 481, 1908
Krüger, C. J., & Foucart, F. 2020, PhRvD, 101, 103002
Kumar, P., Pürrer, M., & Pfeiffer, H. P. 2017, PhRvD, 95, 044039
Kyutoku, K., Okawa, H., Shibata, M., & Taniguchi, K. 2011, PhRvD, 84, 064018
Landry, P., Essick, R., & Chatziioannou, K. 2020, PhRvD, 101, 123007
Landry, P., Essick, R., & Chatziioannou, K. 2021, Nonparametric Constraints on Neutron Star Matter with Existing and Upcoming Gravitational Wave and Pulsar Observations: Weighted Monte Carlo Samples for Neutron Star Observables, v1.0.0, Zenodo, doi:10.5281/zenodo.4678703
Lange, J., O'Shaughnessy, R., & Rizzo, M. 2018, arXiv:1805.10457
Le Tiec, A., & Casals, M. 2021, PhRvL, 126, 131102
Li, T. G. F., Del Pozzo, W., Vitale, S., et al. 2012a, PhRvD, 85, 082003
Li, T. G. F., Del Pozzo, W., Vitale, S., et al. 2012b, JPhCS, 363, 012028
LIGO Scientific Collaboration 2018, LIGO Algorithm Library, doi:10.7935/GT1W-FZ16
LIGO Scientific Collaboration, & Virgo Collaboration 2020a, GCN, 26759, 1
LIGO Scientific Collaboration, & Virgo Collaboration 2020b, GCN, 26807, 1
LIGO Scientific Collaboration, & Virgo Collaboration 2020c, GCN, 26688, 1
Lindblom, L. 2010, PhRvD, 82, 103011
Lindblom, L., & Indik, N. M. 2012, PhRvD, 86, 084003
Lindblom, L., & Indik, N. M. 2014, PhRvD, 89, 064003
Littenberg, T. B., & Cornish, N. J. 2015, PhRvD, 91, 084034
Liu, B., & Lai, D. 2017, ApJL, 846, L11
Liu, B., & Lai, D. 2018, ApJ, 863, 68
Liu, J., McClintock, J. E., Narayan, R., Davis, S. W., & Orosz, J. A. 2008, ApJL, 679, L37
Liu, K., Eatough, R. P., Wex, N., & Kramer, M. 2014, MNRAS, 445, 3115
Luan, J., Hooper, S., Wen, L., & Chen, Y. 2012, PhRvD, 85, 102002
Macleod, D., Urban, A. L., Coughlin, S., et al. 2020, gwpy/gwpy: v2.0.1, Zenodo, doi:10.5281/zenodo.3973364
Magee, R., Fong, H., Caudill, S., et al. 2019, ApJL, 878, L17
Mandel, I., Müller, B., Riley, J., et al. 2021, MNRAS, 500, 1380
Mandel, I., & O'Shaughnessy, R. 2010, CQGra, 27, 114007
Mapelli, M., & Giacobbo, N. 2018, MNRAS, 479, 4391
Matas, A., Dietrich, T., Buonanno, A., et al. 2020, PhRvD, 102, 043023
McKernan, B., Ford, K. E. S., & O'Shaughnessy, R. 2020, MNRAS, 498, 4088
Meidam, J., Tsang, K., Goldstein, J., et al. 2018, PhRvD, 97, 044033
Messick, C., Blackburn, K., Brady, P., et al. 2017, PhRvD, 95, 042001
Miller, M. C., & Miller, J. M. 2014, PhR, 548, 1
Miller-Jones, J. C. A., Bahramian, A., Orosz, J. A., et al. 2021, Sci, 371, 1046
Mills, C., & Fairhurst, S. 2021, PhRvD, 103, 024042
Mishra, C. K., Arun, K. G., Iyer, B. R., & Sathyaprakash, B. S. 2010, PhRvD, 82, 064010
Morscher, M., Pattabiraman, B., Rodriguez, C., Rasio, F. A., & Umbreit, S. 2015, ApJ, 800, 9
Most, E. R., Papenfort, L. J., Weih, L. R., & Rezzolla, L. 2020, MNRAS, 499, L82
Mukherjee, D., Caudill, S., Magee, R., et al. 2021, PhRvD, 103, 084047
Nathanail, A., Most, E. R., & Rezzolla, L. 2021, ApJL, 908, L28
Neijssel, C. J., Vigna-Gómez, A., Stevenson, S., et al. 2019, MNRAS, 490, 3740
Neijssel, C. J., Vinciguerra, S., Vigna-Gomez, A., et al. 2021, ApJ, 908, 118
Ng, K. K. Y., Vitale, S., Zimmerman, A., et al. 2018a, PhRvD, 98, 083007
Ng, K. K. Y., Wong, K. W. K., Broadhurst, T., & Li, T. G. F. 2018b, PhRvD, 97, 023012
Nguyen, P., Schofield, R. M. S., Effler, A., et al. 2021, Environmental Noise in Advanced LIGO Detectors, arXiv:2101.09935
Nissanke, S., Holz, D. E., Hughes, S. A., Dalal, N., & Sievers, J. L. 2010, ApJ, 725, 496
Nitz, A., Harry, I., Brown, D., et al. 2019a, gwastro/pycbc: PyCBC Release v1.15.2, Zenodo, doi:10.5281/zenodo.3596447
Nitz, A. H., Capano, C., Nielsen, A. B., et al. 2019b, ApJ, 872, 195
Nitz, A. H., Capano, C. D., Kumar, S., et al. 2021, arXiv:2105.09151
Nitz, A. H., Dal Canton, T., Davis, D., & Reyes, S. 2018, PhRvD, 98, 024050
Nitz, A. H., Dent, T., Dal Canton, T., Fairhurst, S., & Brown, D. A. 2017, ApJ, 849, 118
Nitz, A. H., Dent, T., Davies, G. S., et al. 2020a, ApJ, 891, 123
Nitz, A. H., Dent, T., Davies, G. S., & Harry, I. 2020b, ApJ, 897, 169
Orosz, J. A., Jain, R. K., Bailyn, C. D., McClintock, J. E., & Remillard, R. A. 1998, ApJ, 499, 375
Orosz, J. A., McClintock, J. E., Aufdenberg, J. P., et al. 2011, ApJ, 742, 84
Orosz, J. A., Steeghs, D., McClintock, J. E., et al. 2009, ApJ, 697, 573
O'Shaughnessy, R., Belczynski, K., & Kalogera, V. 2008, ApJ, 675, 566
O'Shaughnessy, R., Kalogera, V., & Belczynski, K. 2010, ApJ, 716, 615
Ossokine, S., Buonanno, A., Marsat, S., et al. 2020, PhRvD, 102, 044055
Owen, B. J., & Sathyaprakash, B. S. 1999, PhRvD, 60, 022002
Özel, F., Psaltis, D., Narayan, R., & McClintock, J. E. 2010, ApJ, 725, 1918
Pannarale, F. 2013, PhRvD, 88, 104025
Pannarale, F., Tonita, A., & Rezzolla, L. 2011, ApJ, 727, 95
Paschalidis, V., Ruiz, M., & Shapiro, S. L. 2015, ApJL, 806, L14
Portegies Zwart, S. F., & McMillan, S. L. W. 2000, ApJL, 528, L17
Pratten, G., García-Quirós, C., Colleoni, M., et al. 2020a, arXiv:2004.06503
Pratten, G., Husa, S., Garcia-Quiros, C., et al. 2020b, PhRvD, 102, 064001
Pratten, G., Schmidt, P., Buscicchio, R., & Thomas, L. M. 2020c, PhRvR, 2, 043096
Price-Whelan, A. M., Sipőcz, B. M., Günther, H. M., et al. 2018, AJ, 156, 123
Privitera, S., Mohapatra, S. R. P., Ajith, P., et al. 2014, PhRvD, 89, 024003
Pürrer, M. 2016, PhRvD, 93, 064041
Qin, Y., Marchant, P., Fragos, T., Meynet, G., & Kalogera, V. 2019, ApJL, 870, L18
Racine, E. 2008, PhRvD, 78, 044021
Rantsiou, E., Kobayashi, S., Laguna, P., & Rasio, F. A. 2008, ApJ, 680, 1326
Rastello, S., Mapelli, M., Di Carlo, U. N., et al. 2020, MNRAS, 497, 1563
Rhoades, C. E., & Ruffini, R. 1974, PhRvL, 32, 324
Robitaille, T. P., Tollerud, E. J., Greenfield, P., et al. 2013, A&A, 558, A33
Rodriguez, C. L., Zevin, M., Pankow, C., Kalogera, V., & Rasio, F. A. 2016, ApJL, 832, L2
Romero-Shaw, I. M., Farrow, N., Stevenson, S., Thrane, E., & Zhu, X.-J. 2020a, MNRAS, 496, L64
Romero-Shaw, I. M., Talbot, C., Biscoveanu, S., et al. 2020b, MNRAS, 499, 3295
Roy, S., Sengupta, A. S., & Ajith, P. 2019, PhRvD, 99, 024048
Roy, S., Sengupta, A. S., & Thakor, N. 2017, PhRvD, 95, 104045
Sachdev, S., Caudill, S., Fong, H., et al. 2019, arXiv:1901.08580
Safarzadeh, M., Ramirez-Ruiz, E., & Berger, E. 2020, arXiv:2001.04502
Salpeter, E. E. 1955, ApJ, 121, 161
Santamaría, L., Ohme, F., Ajith, P., et al. 2010, PhRvD, 82, 064016
Santoliquido, F., Mapelli, M., Bouffanais, Y., et al. 2020, ApJ, 898, 152
Sarin, N., & Lasky, P. D. 2021, GReGr, 53, 59
Schmidt, P., Ohme, F., & Hannam, M. 2015, PhRvD, 91, 024043
Schutz, B. F. 1986, Natur, 323, 310
Shibata, M., & Taniguchi, K. 2008, PhRvD, 77, 084015

Shibata, M., Zhou, E., Kiuchi, K., & Fujibayashi, S. 2019, PhRvD, 100, 023015
Silsbee, K., & Tremaine, S. 2017, ApJ, 836, 39
Singer, L. P., & Price, L. 2016, PhRvD, 93, 024013
Sipior, M. S., & Sigurdsson, S. 2002, ApJ, 572, 962
Smith, G. P., Berry, C., Bianconi, M., et al. 2017, in IAU Symp. 338, Gravitational Wave Astrophysics: Early Results from Gravitational Wave Searches and Electromagnetic Counterparts, ed. G. González & R. Hynes (Cambridge: Cambridge Univ. Press), 98
Smith, R. J. E., Ashton, G., Vajpeyi, A., & Talbot, C. 2020, MNRAS, 498, 4492
Soni, S., Austin, C., Effler, A., et al. 2020, CQGra, 38, 025016
Soni, S., Berry, C. P. L., Coughlin, S. B., et al. 2021, arXiv:2103.12104
Speagle, J. S. 2020, MNRAS, 493, 3132
Stachie, C., Coughlin, M. W., Dietrich, T., et al. 2021, arXiv:2103.01733
Stegmann, J., & Antonini, F. 2021, PhRvD, 103, 063007
Stevenson, S., Berry, C. P. L., & Mandel, I. 2017, MNRAS, 471, 2801
Stovall, K., Freire, P. C. C., Chatterjee, S., et al. 2018, ApJL, 854, L22
Sun, L., Goetz, G., Kissel, J., et al. 2020, CQGra, 37, 225008
Talbot, C., & Thrane, E. 2017, PhRvD, 96, 023012
Tang, P. N., Eldridge, J. J., Stanway, E. R., & Bray, J. C. 2020, MNRAS, 493, L6
Tews, I., Pang, P. T. H., Dietrich, T., et al. 2021, ApJL, 908, L1
Thompson, J. E., Fauchon-Jones, E., Khan, S., et al. 2020, PhRvD, 101, 124059
Tiwari, V. 2018, CQGra, 35, 145009
Urban, A. L. 2016, PhD thesis, Univ. Wisconsin Milwaukee
Usman, S. A., Nitz, A. H., Harry, I. W., et al. 2016, CQGra, 33, 215004
Vajente, G., Huang, Y., Isi, M., et al. 2020, PhRvD, 101, 042003
Valsecchi, F., Glebbeek, E., Farr, W. M., et al. 2010, Natur, 468, 77
Veitch, J., Raymond, V., Farr, B., et al. 2015, PhRvD, 91, 042003
Venumadhav, T., Zackay, B., Roulet, J., Dai, L., & Zaldarriaga, M. 2019, PhRvD, 100, 023011
Venumadhav, T., Zackay, B., Roulet, J., Dai, L., & Zaldarriaga, M. 2020, PhRvD, 101, 083030
Viets, A. D., Wade, M., Urban, A. L., et al. 2018, CQGra, 35, 095015
Vitale, S., Gerosa, D., Haster, C.-J., Chatziioannou, K., & Zimmerman, A. 2017a, PhRvL, 119, 251103
Vitale, S., Lynch, R., Raymond, V., et al. 2017b, PhRvD, 95, 064053
Vitale, S., Lynch, R., Sturani, R., & Graff, P. 2017c, CQGra, 34, 03LT01
Vitale, S., Lynch, R., Veitch, J., Raymond, V., & Sturani, R. 2014, PhRvL, 112, 251101
Weltman, A., Bull, P., Camera, S., et al. 2020, PASA, 37, e002
Wong, T.-W., Valsecchi, F., Fragos, T., & Kalogera, V. 2012, ApJ, 747, 111
Wysocki, D., Gerosa, D., O'Shaughnessy, R., et al. 2018, PhRvD, 97, 043014
Wysocki, D., Lange, J., & O'Shaughnessy, R. 2019, PhRvD, 100, 043012
Ye, C. S., Fong, W.-F., Kremer, K., et al. 2020, ApJL, 888, L10
Yunes, N., & Pretorius, F. 2009, PhRvD, 80, 122003
Zackay, B., Dai, L., Venumadhav, T., Roulet, J., & Zaldarriaga, M. 2019a, arXiv:1910.09528
Zackay, B., Venumadhav, T., Dai, L., Roulet, J., & Zaldarriaga, M. 2019b, PhRvD, 100, 023007
Zappa, F., Bernuzzi, S., Pannarale, F., Mapelli, M., & Giacobbo, N. 2019, PhRvL, 123, 041102
Zevin, M., Spera, M., Berry, C. P. L., & Kalogera, V. 2020, ApJL, 899, L1
Zhao, X., Gou, L., Dong, Y., et al. 2021, ApJ, 908, 117
Zhu, X., Thrane, E., Osłowski, S., Levin, Y., & Lasky, P. D. 2018, PhRvD, 98, 043002
Ziosi, B. M., Mapelli, M., Branchesi, M., & Tormen, G. 2014, MNRAS, 441, 3703